Mixed Convection Phenomena Inside a Simplified Tyre Geometry

Thesis submitted in partial fulfilment of the requirements for the degree of

Master of Research (Science and Engineering)

By James Slaughter

Faculty of Science and Engineering

supervised by
Dr. Sammy Diasinos

Submitted on: May 1, 2018

Abstract

To further current methodology and understanding regarding heat transfer in motorsport tyres, RANS/URANS methodologies were created and compared to investigate natural and mixed convection phenomena in a simplified tyre geometry subject to a thermal gradient from rim surface to tyre crown. At a Rayleigh Number (Ra) of 5.02 $\times 10^6$ natural convection phenomena were investigated and variation in outer cylinder Nusselt Number (Nu) was quantified. With rotational effects at a higher Rayleigh Number of 1.094×10^7, a weak correlation between Reynolds Number (Re) and outer cylinder Nu was found with 21% variation across the whole Re range ($4.851 \times 10^5 < Re < 1.698 \times 10^6$), with most variation occurring at lower Re.

Further, a RANS and URANS methodology were compared for resolution of Natural Convection phenomena. Steady-State and Transient Implicit solvers were compared with minimal variation in results but the transient solver taking 0.709% longer per iteration and 51.06% longer to converge. The transient methodology showed promise however as they did not encounter similar stability issues as steady-state solutions at higher Ra.

Acknowledgments

There are a number of key individuals that have assisted in both the undertaking of my Masters of Research and the preparation and completion of this thesis.

Firstly, to my supervisor Dr Sammy Diasinos. Thank you for your significant assistance with the completion of all aspects of my Masters. I have learnt a significant amount over the past 18 months thanks to your guidance and for that I am extremely grateful. In addition, the discussions about Formula 1 and aerodynamics in general and your insights have been much valued.

Thanks must be given to Matteo Lombardi and Scuderia Toro Rosso. Matteo, I appreciate the work you have put in over the past year and the ideas and the back and forth discussion we have had through email. Thank you for the frank discussions and suggesting this topic. I'm extremely grateful for this opportunity.

I must thank Riccardo Pagliarella for both the many conversations about career, my Masters project or any number of esoteric topics that have come up. Your willingness to help out with regards to introductions or advice on technical matters have been invaluable and my thesis would not be at the same standard without it. Thanks must also be extended for the introduction to Matteo.

To NCI and AWS for the assistance with computational resources, my thanks are also given. All simulations presented in this thesis were performed on either Raijin or AWS and completion of this project would not have been possible otherwise.

A thank you must be extended to my colleagues, Sajjad Saleh and Andre Aquino, whom I have shared my Masters experience with as well as Liang Yu and Tim Jellema. Thank you for the all the educational or non-educational related discussions throughout the year.

Finally to all of my friends and family: thank you for providing the much needed ear when I am stressed about a submission or for just being a chance to get away. You have all been a breath of fresh air and your company has been cherished.

DECLARATION

I, James Slaughter, declare all work presented in this thesis is my own and any significant contribution from another has been documented and referenced as such. None of this document has been submitted for a degree at any other university and to the best of my knowledge this thesis contains no material previously published or written by another person except where reference has been made.

Signature : 

CandidateName : James Slaughter

Date : 01/05/2018

Abbreviations

RANS	Reynolds Averaged Navier Stokes
EVM	Eddy Viscosity Model
F1	Formula 1
Nu	Nusselt Number
MUSCL	Monotonic Upwind Scheme for Conservation Laws
TVD	Total Variation Diminishing
SIMPLE	Semi-Implicit Method for Pressure Linked Equations
CFD	Computational Fluid Dynamics
CFL	Courant-Friedrichs-Lewy Number
NCI	National Computational Infrastructure
AWS	Amazon Web Service
CPU	Central Processing Unit
RAM	Random Access Memory
GPU	Graphics Processing Unit
GB	Gigabyte
HPC	High Performance Computing
RNG	Renormilisation Group
LES	Large Eddy Simulation
EASM	Explicit Algebraic Stress Model
URANS	Unsteady Reynolds Averaged Navier Stokes
Re	Reynolds Number
Ra	Rayleigh Number
Pr	Prandtl Number
2D	2 Dimensional
3D	3 Dimensional

Nomenclature

α	Thermal Diffusivity
β	Thermal Expansion Coefficient
c_p	Specific Heat Capacity
δ_{ij}	Kronecker Delta
ϵ	Rate of Dissipation of Turbulent Kinetic Energy
C_μ	Epsilon Coefficient = 0.09
η	Radius Ratio
g	Gravitational Acceleration
h	Convective Heat Transfer Coefficient
I	Turbulence Intensity
k	Thermal Conductivity
k	Turbulent Kinetic Energy
l	Length Scale
L	Characteristic Length
λ	Aspect Ratio
M_w	Molecular Weight
μ_t	Turbulent Viscosity
ν	Kinematic Viscosity
ω	Angular Velocity
p	Pressure
P_k	Turbulent Production Term
p_{op}	Operating Pressure
R	Universal Gas Constant
ρ	Density
Ri	Inner Radius
Ro	Outer Radius
S_{ij}	Strain Rate Tensor
T	Temperature
τ_{ij}	Reynolds Stress Tensor
ΔT	Change in Temperature
Δt	Timestep
w	Span Length
z	Spanwise Distance

Contents

List of Figures

List of Tables

Chapter 1

Introduction and Background

Formula 1 exhibits a large and diverse range of stakeholders with substantial global investments from automotive manufacturers, technology specialists and sponsoring organisations alike. Teams of up to 1500 people and budgets exceeding $400 million (USD) compete for both drivers and constructors championships. Figure 1.1 exhibits a small piece of the engineering and logistical effort Teams and individual engineers search for any competitive or technical advantage to outperform on a race weekend. Tyres are one such area where teams invest substantial engineering resources.

Figure 1.1 has been removed due to copyright policy. It can be accessed via:

https://www.motorsport.com/f1/news/hamilton-says-mexican-gp-track-is-crazy-slippery/

https://www.racefans.net/wp-content/uploads/2016/10/mercedes-2016-3.jpg

Figure 1.1: Left: Mercedes F1 Car with a Rear Brake Fire Note. Adapted [reprinted] from "Hamilton says Mexican GP track is crazy slippery" by Motorsport Network 2015, Retrieved from https://www.motorsport.com/f1/news/hamilton-says-mexican-gp-track-is-crazy-slippery/ 2015 by Motorsport Network.

Right: Mercedes Team Photo Adapted [reprinted] from "Mercedes F1 Team Photo" by Collantine Media 2016, Retrieved from https://www.racefans.net/wp-content/uploads/2016/10/mercedes-2016-3.jpg 2016 by Collantine Media

Tyres are complex systems having one of the most significant effects on overall handling and performance. They exhibit viscoelastic characteristics and are further influenced by a considerable array of variables. Notable engineers such as Hans Pacejka have pioneered the efforts to understand the tyre. Pacejka and Bakker (1992) championed the development of empirical models, penned the 'Magic Formula', that take experimental tyre data for slip angle/ratio versus normal load for several different conditions. By varying inclination angle, tyre pressure, temperature; this data allows engineers to gain an indication of the performance

of the tyre for a given set of operating conditions. These models demonstrate a significant variance in performance across a variety of input conditions, but most notably to this work, a variation in load (lateral or longitudinal) for both inflation pressure and temperature.

A pneumatic tyre is essentially a carcass, composed of various compounds of rubber intertwined with plys of steel belts (Figure 1.2). This is placed on a rim, retained by a lip (the bead), and filled with a gas (typically air or nitrogen). Formula 1, in particular, utilises a number of compounds for both dry and wet weather running.

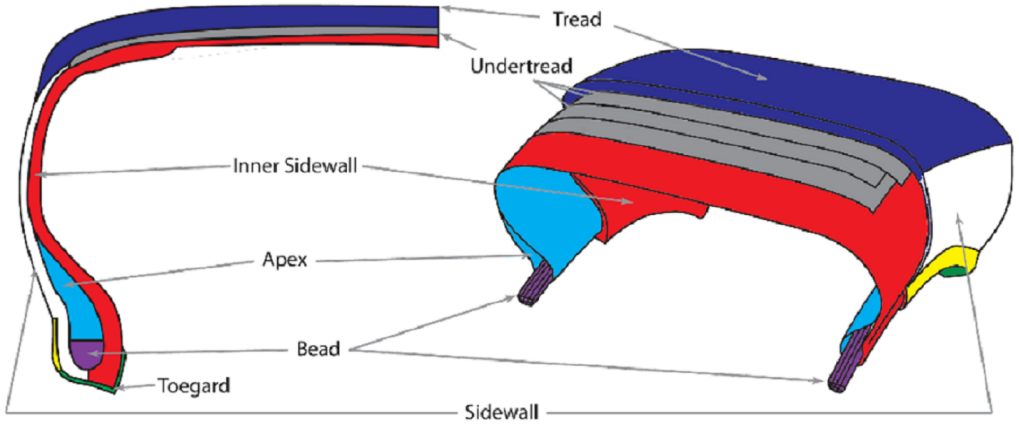

Figure 1.2: Cross Section of a Tyre Construction Note. Adapted [reprinted] from "Optimization of reinforcement turn-up effect on tyre durability and operating characteristics for racing tyre design" X. Yang and O. A. Olatunbosun, 2011, Journal of Materials and Design, 35, 798-809, 2011 by "Elsevier Ltd."

Any variation in tyre performance is significant dictating large engineering efforts to understand the influence of various operating conditions. Teams must ensure both the longevity of the tyre but also must attempt to extract maximum instantaneous potential performance. The operating window of a race tyre is extremely narrow often $5°C$ or smaller (Pappone, 2017). Operating outside optimal temperature parameters can lead to detrimental tyre behaviours, the possibility of graining or uneven wear patterns with tread temperatures too low or high respectively. It is therefore of utmost importance that engineers understand heat transfer phenomena. In motorsport applications, brakes are the most significant source of thermal energy.

The brake rotors on an F1 car reach surface temperature peaks of roughly 1000-1200°C over the duration of a race (Brembo, 2018; Sprot, 2013) with braking decelerations of 6.08g and thermal loads ranging up to 22.2 kJ observed. Whilst, some of this thermal energy is dissipated through the brake shroud and outboard of the wheel, a large amount also convects and radiates into the rim. From here, a significant analysis must be conducted to investigate the manner and proportion of heat transfer between the rim and the tyre crown in order to further increase the performance limits and longevity of the tyre compound. Figure 1.3 shows the complexity of the wheel internals.

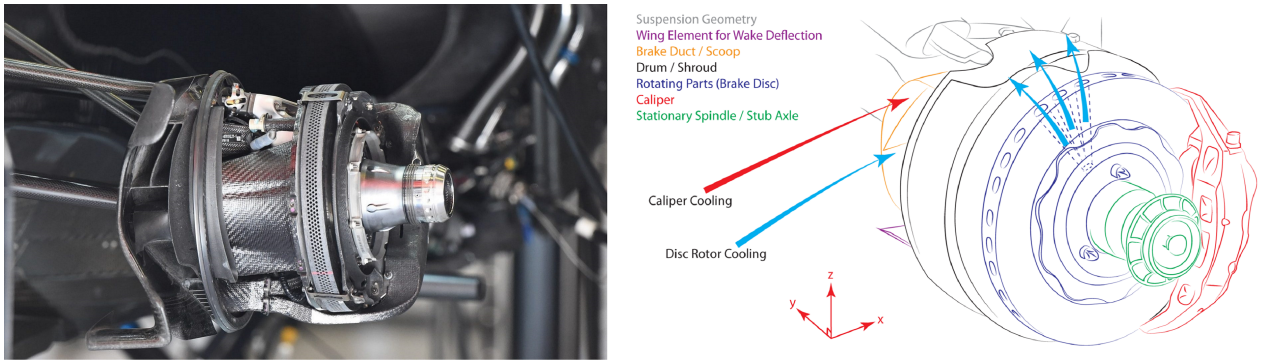

Figure 1.3: Left: Brake Detail Note. Adpated [reprinted] from "Brakes" by Formula 1 World Championship Limited, 2015. Retrieved from "https://www.formula1.com/en/championship/inside-f1/understanding-f1-racing/Brakes.html", 2015 by Formula 1 World Championship Limited.

Right: Diagram of Brake Assembly. Note. Adapted [reprinted] from "Open-Wheel Aerodynamics: Effect of Tyre Deformation and Internal Flow" by A. J. Sprot, 2013, 2013 by Sprot.

Chalingé (2011) demonstrates the implication of temperature on lateral load by curve-fitting a model to empirical tyre data. Figure 1.4 shows the effects of thermal variation on a -20 to 20 to -20° Slip Angle sweep. Whilst this model only accounts for heating from friction/adhesion or shearing of the rubber carcass and the road through the tyre contact patch, it still demonstrates fairly significant behaviours, purely dependent on carcass temperature. The model and experimental data both show a higher peak lateral grip, with a gradual decline after a peak of roughly 6°. Tyres also exhibit either temperature effects or hysteresis on the reverse pass with lower values for the measured lateral forces at the same slip angles than the modelled case. In either scenario, the temperature of the tyre carcass is a critical variable that must be closely controlled and has substantial performance implications.

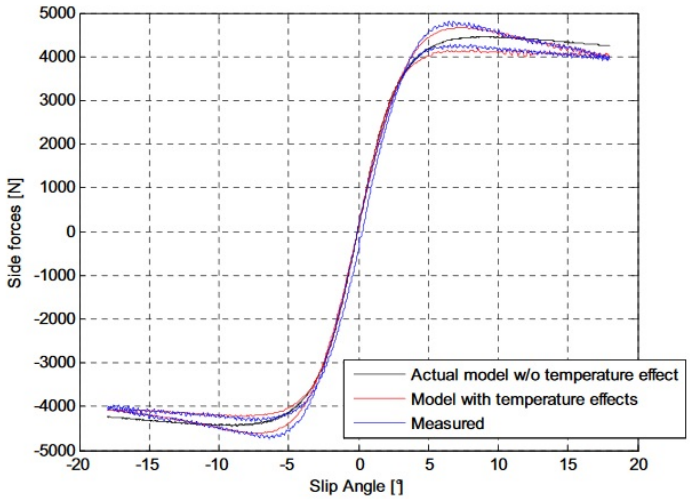

Figure 1.4: Modelled Slip Angle v Normal Load Sweep With and Without Temperature Effects. Note. Adapted [reprinted] from "Tire thermal analysis and modeling" by S. Chalingé, 2011, 2011 by Chalingé

Formula 1 is heavily regulated to protect stakeholder investments and present a relatively level playing field for all competitors. This includes aerodynamic development in which the sporting

regulations prohibit excessive use of wind tunnel or computational development of components (FIA, 2017). With an absolute limit of 25 teraFLOPS imposed on all instantaneous numerical aerodynamic studies trade-offs between accuracy, simulation robustness and economy are made.

1.1 Aims and Objectives

This thesis investigates a novel methodology to resolve convection phenomena in an "F1 style" pneumatic tyre. It allows for the investigation and the characterisation of the impacts of various heat transfer phenomena, aid in the development of future tyre temperature prediction and direct future development areas.

Therefore, the aims of this work are presented as follows:

- Create a methodology to resolve time-averaged phenomena natural convection phenomena within a pneumatic tyre
- Investigate the applicability of RANS/URANS Methodologies to Convection Phenomena
- Investigate the implication of Reynolds Number $(10^6 - 10^7)$ on flow phenomena at a constant Rayleigh Number
- Investigate the implication of Rayleigh Number $(10^6 - 10^7)$ on flow phenomena
- Make recommendations for future development directions

Chapter 2

Literature Review

Buoyant or Natural Convection is historically a topic of significant scientific interest. Of more relevance, natural convection applied to concentric cylindrical annuli has also been studied extensively. Studies including Kuehn and Goldstein (1978) and Bishop (1988) utilised experimental methods to gain an understanding of intrinsic flow phenomena; whilst both higher-order (Padilla & Silvira-Neto, 2008) and RANS methodologies (Char & Hsu, 1998; Kenjereš & Hanjalić, 1995) have been conducted in conjunction to further investigate the specifics of the problem. The following section will outline and present the relevant literature.

Natural Convection phenomena in an annulus is a representation of a non-rotating tyre i.e. a car sitting on a grid at the start of a race. Most works presented in the current literature review, whilst evaluating similar geometry, use different geometric relationships and non-dimensional parameters. Most previous simulation work has assumed symmetrical and/or 2D flow which may not best represent flow inside a tyre.

2.1 Theoretical Modelling

Natural Convection occurs primarily due to a change in density in a fluid, with temperature and density being inversely proportional from the ideal-gas law, i.e:

$$p = \rho RT \tag{2.1}$$

Temperature gradients, cause a change in density, which through an additional body force term in the Navier-Stokes Momentum Equation causes additional flux or bulk movement of the fluid. A number of key dimensionless parameters exist that define the fluid flow for natural convection. Firstly, the Prandtl Number is defined as the ratio of momentum diffusivity to thermal diffusivity. Prandtl Number varies for a given fluid due to temperature and pressure. However, for a large array of gases Prandtl Number is close to constant over a large array of temperatures and pressures. For example, Prandtl Number of nitrogen only varies by $\approx 10\%$

over 1200K at 1 atmosphere ("Thermophysical Properties: Nitrogen at 1 atm", 2010). Bishop (1988) defines the Prandtl Number as:

$$Pr = \frac{\nu}{\alpha} \tag{2.2}$$

The Rayleigh Number signifies the relationship between buoyant forces and viscous forces in a given flow field (Bishop, 1988):

$$Ra = \frac{g\beta\Delta T L^3}{\nu\alpha} \tag{2.3}$$

Finally, the Nusselt Number is defined as the ratio of convective to conductive heat transfer:

$$Nu = \frac{hL}{k} \tag{2.4}$$

2.2 Natural Convection in a Horizontal Concentric Cylindrical Annulus

Concentric and non-concentric cylindric annuli have been investigated by both numerical (Char & Hsu, 1998) and empirical methods (Kuehn & Goldstein, 1978). Figure 2.1 shows an example from Desai and Vafai (1994) visualises the basic form that has been utilised for most of these works.

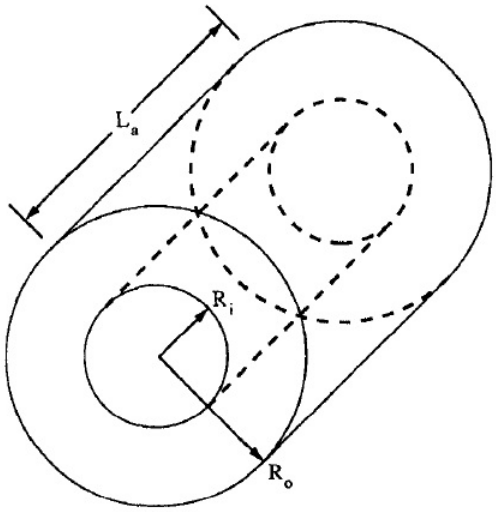

Figure 2.1: Schematic of the Numerical Domain. Adapted [reprinted] from "An investigation and comparative analysis of two- and three-dimensional turbulent natural convection in a horizontal annulus" by C. P Desai and K. Vefai, International Journal of Heat Mass Transfer, 94, 2475-2504. 1994 by Elsevier Ltd.

A number of key geometric relationships are necessary. Firstly, the radii of the inner and outer cylinders are defined as R_i and R_o respectively and temperatures defined in a similar fashion i.e. T_i and T_o. Secondly, the radius ratio and aspect ratio are defined as, $\eta = \frac{R_o}{R_i}$ and $\lambda = \frac{L_a}{L}$,

where L is the gap width or length scale, $L = R_o - R_i$.

Whilst for simplification's sake the internal geometry of a tyre can be represented as a uniform annulus; as shown in Figure 1.2, it is in reality not the case. A tyre geometry deforms significantly under applied normal load and/or slip angle and elongates with increase angular velocity as described by Sprot (2013). The contact patch and applied shear distribution drastically change the shape of the lower section of the tyre. Figure 2.2 shows a simplistic representation of the side wall compression due to normal load application and rotation.

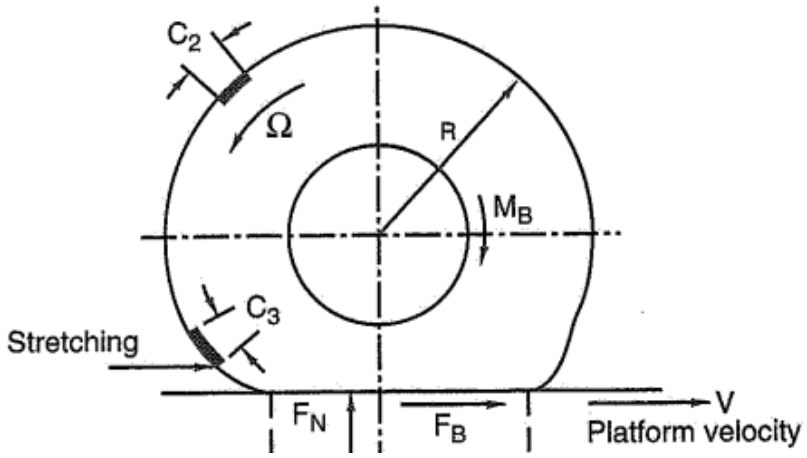

Figure 2.2: Deformed Tyre Cross Section. Adapted [reprinted] from "Race Car Vehicle Dynamics" by W. F Milliken and D.L Milliken, 1995, Warrendale, PA: SAE International. 1995 by SAE International

2.3 Experimental Works

Kuehn and Goldstein (1978) conducted a pivotal experimental study investigating natural convection in an annulus utilising concentric and eccentric annuli with Rayleigh Numbers 1 $\times 10^2$ - 1 $\times 10^7$ placing the domain within all flow regimes. i.e. laminar, transitional and turbulent. The crux of this particular study was to investigate the implications of eccentricity (implication of moving the inner cylinder) on internal heat transfer values. By varying both the pressure and temperature difference across the chamber the authors quantified the flow field over a large Rayleigh Number range. Using of a Mach-Zehnder interferometer the flow field was both visualised and quantified. Consequently, Kuehn and Goldstein (1978) presented interferograms, time-averaged dimensionless temperature distributions, local heat transfer coefficients and a correlation equation for average Nu versus Rayleigh Number. The authors demonstrate that flow features witnessed are heavily dependent on the Rayleigh Number.

Figure 2.3 shows instantaneous interferograms for concentric annuli varying Rayleigh Number. Up to Figure 2.3 (d) the interferograms indicate a laminar flow field with little irregularity in

the edge of the fringe patterns. Figure 2.3 (e) shows significant variation in the fringe shifts in the upper section of the thermal plume and the outer cylinder boundary layer with the whole plume showing similar properties in Figure 2.3 (f), suggesting the development of turbulent characteristics around Ra $= 1 \times 10^7$. Kuehn and Goldstein (1978) note plume and outer cylinder boundary layer oscillation earlier than the development of turbulent characteristics, however, suggesting that unsteady behaviour begins as early as 5×10^5 and lack of any oscillation above Ra $= 1.5 \times 10^6$.

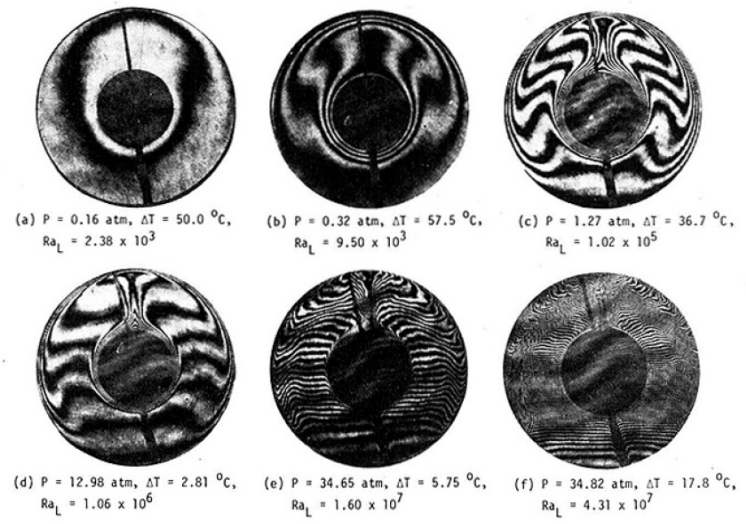

Figure 2.3: Instantaneous Interferograms Showing Implications of Increasing Rayleigh Number. Adapted [reprinted] from "An Experimental Study of Natural Convection Heat Transfer in Concentric and Eccentric Horizontal Cylindrical Annuli" T. H. Kuehn and R. J. Goldenstein, 1978, Journal of Heat Transfer, 100, 635-640. 1978 by American Society of Mechanical Engineers.

Additionally, the study established (through a combination of Figure 2.4 and the previous interferograms) that the largest heat transfer values occur in the region of the plume. These further show an almost stagnant region above angular positions of 150° with little variation between $150 < \theta < 180°$ (Kuehn & Goldstein, 1978).

Bishop (1988) further substantiated the impact of normalized expansion coefficient ($\beta\Delta T$) on heat transfer rates, conducting an empirical study using Helium up to a significantly higher Rayleigh number (6×10^6 - 2×10^9) for a radius ratio of 3.36. By varying the normalized expansion coefficient and maintaining a constant Prandtl Number (0.688) Bishop found significant variance in equivalent conductivity. Figure 2.5 demonstrates the development and the variance caused by changing the expansion coefficient and the deviation in comparison to other previously proposed correlation equations.

Finally, Kuehn and Goldstein presented a study comparing empirical methodologies to a numerical study conducted with finite difference techniques (Kuehn & Goldstein, 1976). In contrast with most of the previous experimental studies, Kuehn and Goldstein (1976) investigated higher

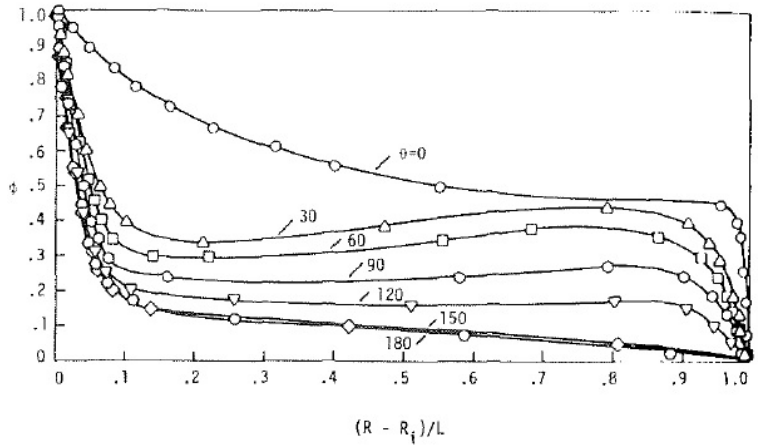

Figure 2.4: Normalised Temperature Distribution Ra = 2.51 $\times 10^6$. Adapted [reprinted] from "An Experimental Study of Natural Convection Heat Transfer in Concentric and Eccentric Horizontal Cylindrical Annuli" T. H. Kuehn and R. J. Goldenstein, 1978, Journal of Heat Transfer, 100, 635-640. 1978 by American Society of Mechanical Engineers.

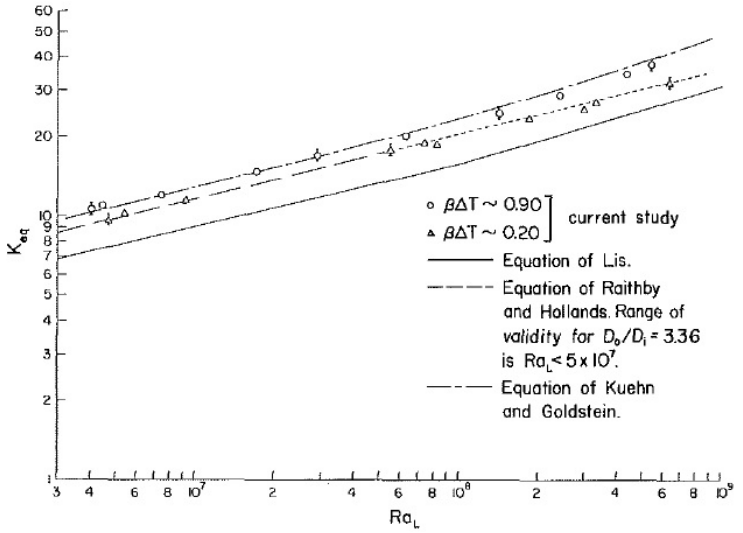

Figure 2.5: Variation of Equivalent Conductivity with $\beta\Delta T$. Adapted [reprinted] from "Heat Transfer by Natural Convection of Helium Between Horizontal Isothermal Concentric Cylinders at Cryogenic Temperature" by E. H. Bishop, 1988, Journal of Heat Transfer, 110, 109-115. 1998 by American Society of Mechanical Engineers.

Prandtl Number fluids (e.g. water as opposed to gases in previous literature). The experimental results suggest that a steady regime exists for a larger array of Rayleigh Numbers for fluids with increasing Prandtl Number. However, this study only investigated lower Rayleigh Number ranges i.e. up to 1 $\times 10^5$.

2.4 Numerical Studies

Some conjecture exists in the presented literature on the effect of experimental conditions on the production of correlation equations (Kenjereš & Hanjalić, 1995). Figure 2.5 shows an ex-

ample of this, with 4 heat transfer correlation present that all significantly differ based on flow conditions. Kenjereš and Hanjalić (1995) further suggest that a consensus or a usable correlation equation would be difficult and unlikely to be generated. As such, numerical modelling is hypothesised as an alternative (Kenjereš & Hanjalić, 1995).

One of the first numerical studies Farouk and Güçeri (1982) shows the effects of Rayleigh number on turbulent quantities. Concluding a similar result to Kuehn and Goldstein (1978) at a Rayleigh number of 1×10^7, the authors state that due to lack of significant values of turbulent viscosity outside the upper half of the annulus the flow is only partially turbulent. The authors go on to extend this work and demonstrate the implications of buoyancy on turbulent quantities. Values for k are up to 2 orders of magnitude higher in both the plume and near the wall than the stagnant region at the bottom of the annulus, demonstrating that buoyancy and shear have a significant influence on turbulent quantity production. The study further suggests both that the finer-grids are required for higher Ra as the boundary layer thins with increasing Ra and the use of wall functions could decrease the required computational resources.

Francis et al. (2002) showed the applicability of 2 equation Eddy viscosity models by simulating a 2D annulus with symmetry from $8.9 \times 10^5 < Ra < 5.3 \times 10^9$. Authors of this particular study achieved convergence by the use of extremely low under-relaxation factors (noting as low as 0.01 in the higher Rayleigh Number cases), exotic pressure interpolation schemes (Body-Force Weighted) and a TVD convection discretisation scheme (MUSCL). Francis, Itamura, S. W., and James (2002) also initialised cases with previously lower-Ra runs and scaling the gravity vector, thus gradually increasing the significance of body forces. Difficulty in resolving the thermal plume in comparison to Kuehn and Goldstein (1978) using the proposed methodology was noted characterised by an overprediction of normalised temperature distribution in the plume. The suggestion is that the modelling of the eddy-diffusivity term, i.e. the under-lying assumption in the RANS models is the cause.

Char and Hsu (1998) attempted to rectify temperature over-prediction in the plume by utilising the Low-Re k-ϵ turbulence model with both the Kato and Launder and Yap modifications. The Yap modification is an additional source term in the ϵ equation that limits the production of large near-wall length scales in any separated or recirculating region. More importantly, the Kato and Launder correction stops the excessive turbulent kinetic energy production in the region directly above the inner cylinder. This is done by changing the production term (P_k in the k equation. The normal model sets $P_k \; \alpha \; \overline{S^2}$ i.e. the production term Pk is proportional to the stress-tensor only. The Kato and Launder correction solves this problem by changing this term to $\overline{S\Omega}$ i.e. changing the production term to be dependent on both the stress and vorticity tensors. The consequence of this is that the vorticity tends to 0 at the region most effected and as such reduces the effect production term and hence resolves more realistic values of k.

Figure 2.6 shows a comparison of the various methodologies utilised by Char and Hsu (1998) and the implication each methodology had on Local Nusselt Number in comparison to Kuehn and Goldstein (1978). The Kato-Modification shows significant improvement for the prediction of Local-Nusselt Number in the region of the thermal plume.

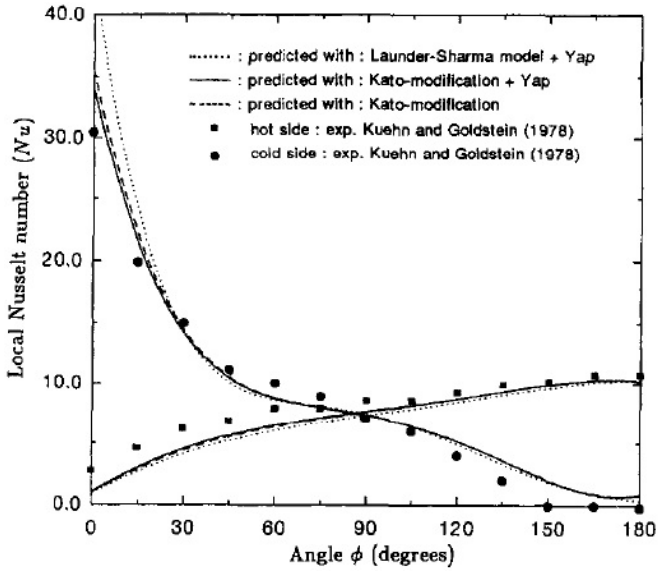

Figure 2.6: Local Nusselt Number Distribution Demonstrating Impact of Kato-Modification. Adapted [reprinted] from "Numerical prediction of turbulent mixed convection in a concentric horizontal rotating annulus with low-Re two-equation models" by M. I. Char and Y. H. Hsu, 1998, International Journal of Heat and Mass Transfer, 110 (12), 1633-1643. 1998 by Elsevier Ltd.

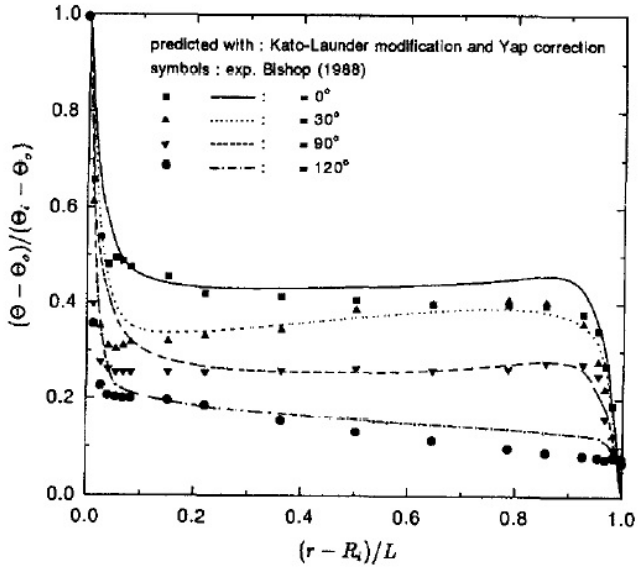

Figure 2.7: Normalised Temperature Distribution and Comparison. Adapted [reprinted] from "Numerical prediction of turbulent mixed convection in a concentric horizontal rotating annulus with low-Re two-equation models" by M. I. Char and Y. H. Hsu, 1998, International Journal of Heat and Mass Transfer, 110 (12), 1633-1643. 1998 by Elsevier Ltd.

In addition to the additional production terms, Char and Hsu (1998) utilised a colocated, finite-volume discretisation and the SIMPLE algorithm for pressure-velocity coupling. Char

and Hsu (1998) also utilised the MUSCL scheme for advective fluxes. Figure 2.7 shows the comparison between time-averaged normalised temperature distributions against Bishop (1988) at a Rayleigh Number of 1.15 $\times 10^9$. The methodology - whilst still over-predicting temperature values in the region of the plume - shows improvements over the methodology employed by Francis et al. (2002). These results suggest that good quantitative agreement between empirical and numerical methodology can be achieved using an implicit pressure-velocity coupling and steady-state methodologies at significant Rayleigh Numbers.

More of note, Desai and Vafai (1994) show the implication of Prandtl Number (0.01<Pr<5000) on heat transfer. Desai and Vafai (1994) found results similar to those previously demonstrated by Kuehn and Goldstein (1976) by visualising a turbulent viscosity decrease with an increase in Pr The conclusion was made that production of turbulent parameters is inversely proportional to Pr and consequently a delay in transition between laminar and turbulent regimes would exist dependent on Pr. Conversely, the paper shows the increase in values for normalised temperature and a reduction in thermal dissipation with increasing Pr. Local heat transfer rates also follow similar trends i.e. increasing Nu with Prandtl Number.

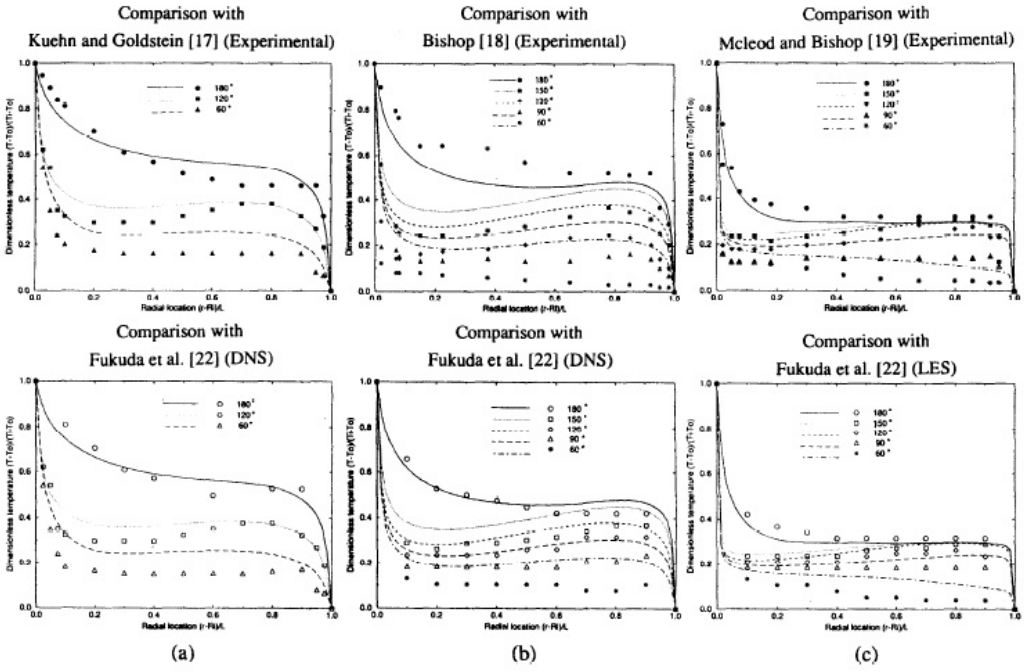

Figure 2.8: RANS Validation. Adapted [reprinted] from "An investigation and comparative analysis of two- and three-dimensional turbulent natural convection in a horizontal annulus" by C. P Desai and K. Vefai, 1994, International Journal of Heat Mass Transfer, 94, 2475-2504. 1994 by Elsevier Ltd.

Desai and Vafai (1994) utilised a wall-modelled approach; whilst the mean temperature profiles provided show an acceptable quantitative comparison with a variety of other numerical and experimental results, all results tended to poorly resolve near-wall flow (Figure 2.8). It is the opinion of the author that this is due to the wall-modelled approach. As a consequence, Figure

2.9 shows the implications on the prediction of local Nu compared to Kuehn and Goldstein (1978). The authors of the paper note the variance of Nu as an observation but do not offer a rationale.

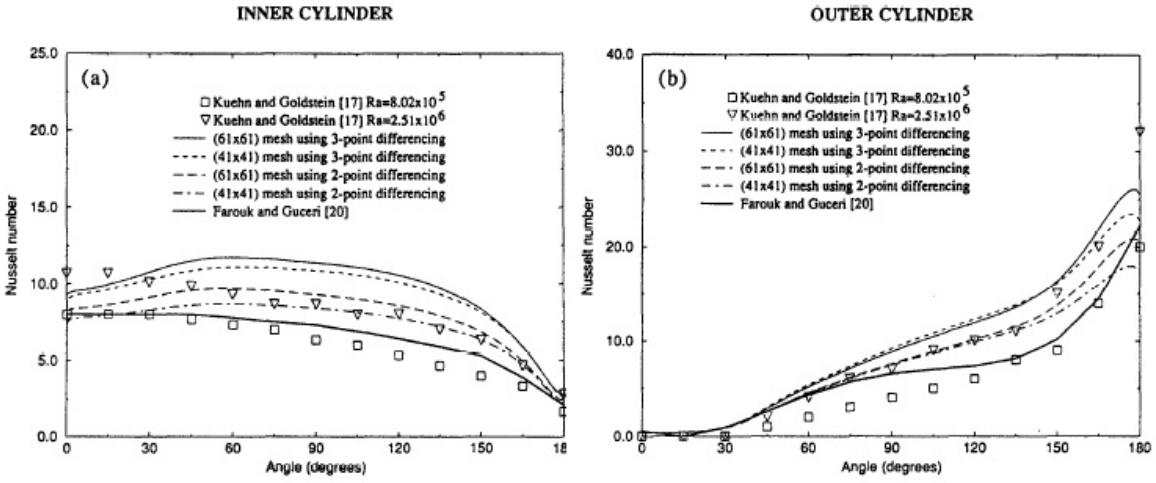

Figure 2.9: Comparison of Local Nusselt Number. Adapted [reprinted] from "An investigation and comparative analysis of two- and three-dimensional turbulent natural convection in a horizontal annulus" by C. P Desai and K. Vefai, International Journal of Heat Mass Transfer, 94, 2475-2504. 1994 by Elsevier Ltd.

Whilst the simulations previous do present a starting point concerning both major flow phenomena and numerical methodologies, all previously cited use a 2D or a 2D symmetrical approach. By assuming a large aspect ratio (as demonstrated by Desai and Vafai (1994)) a core region (for $\lambda > 7.5$) exists making the assumption of two-dimensionality and symmetry within the flow field acceptable. Tyres have significantly lower aspect ratios (for instance $1 < \lambda < 3$) making any 2D simplification questionable.

Kenjereš and Hanjalić (1995) established through the use of an algebraic model for turbulent heat flux, $\overline{\Theta u_i}$, and a low-Re wall treatment, that higher-order treatment is required for more consequential resolution of flow phenomena with large improvements in predicting of flow phenomena at transitional Rayleigh Number ranges. However, Kenjereš and Hanjalić (1995) explain that whilst employing higher-order algebraic models better resolve certain flow features they are significantly more computationally taxing. They further state that single-point closure (i.e. eddy-viscosity models) is able to resolve significant flow phenomena to a satisfactory level.

More recently, Padilla and Silvira-Neto (2008) has modelled the transitional Rayleigh Number regime using Large-Eddy Simulation. By modelling the system as 3D and transient and resolving a significant array of turbulent length scales, significantly more detail about the flow features can be extracted than in RANS models. Figure 2.10 shows the development of instabilities in the radial velocity profile at a probe located mid-gap on the positive vertical axis. Padilla and Silvira-Neto (2008) notes that for buoyant flows in particular, the location of observation has a

strong implication on the behaviour of the flow field. This is supported by the development of turbulence and the fringe patterns seen by Kuehn and Goldstein (1978) in the interferograms at similar Ra.

With radial velocity showing significant chaotic fluctuations at $Ra > 10^5$, effects on other time-resolved flow properties are investigated. Figure 2.11 demonstrates the temporal fluctuation of temperature at the same probe as Figure 2.10 at a Ra value of 1.7 $\times 10^5$. Significantly, whilst radial velocity shows chaotic behaviour temperature shows almost periodic tendencies with spectra showing a defined peak at 2.33Hz, with a secondary peak in the range of 5Hz.

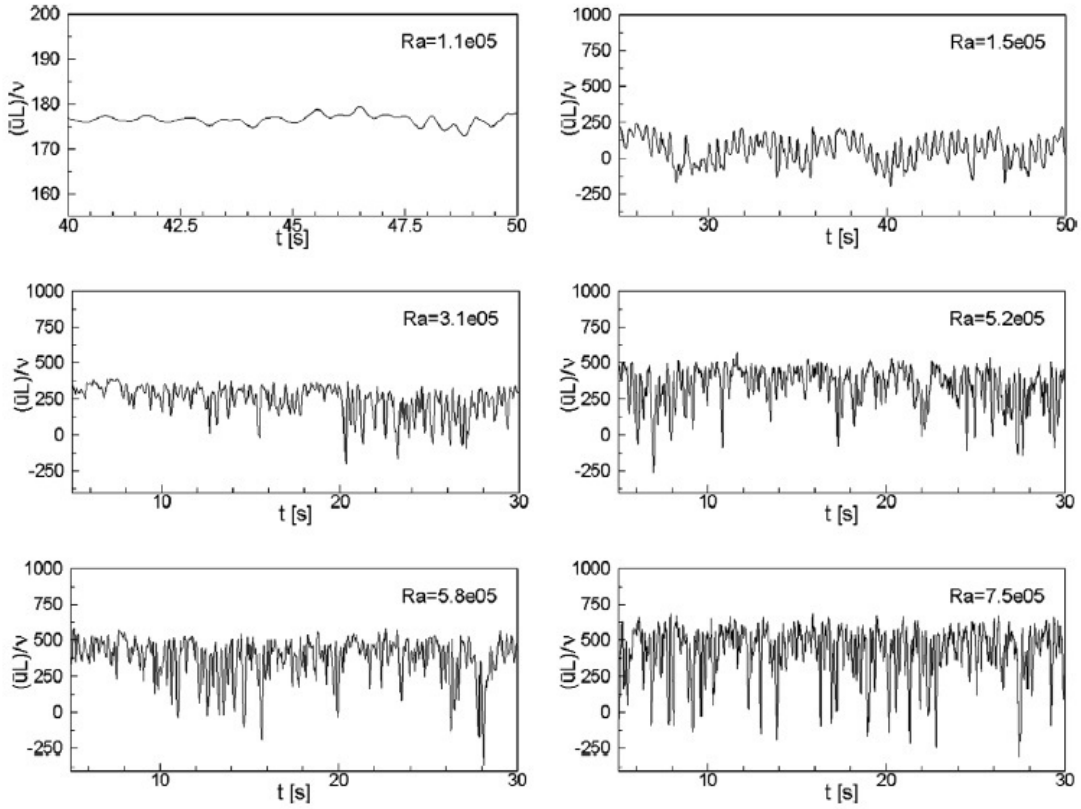

Figure 2.10: Time Resolved Radial Velocity for Different Rayleigh Numbers at Mid-Gap $\phi = 0$. Adapted [reprinted] from "Large-eddy simulation of transition to turbulence in natural convection in a horizontral annular cavity" by E. L. Padilla and A. Silvira-Neto, 2008, International Journal of Heat and Mass Transfer, 51, 3656-3668, 2008 by Elsevier Ltd.

Due to the inherent anisotropic nature of the LES formulation, Padilla and Silvira-Neto (2008) resolved a 3D domain at $\lambda = 2.8$. Figure 2.12 demonstrates the isosurfaces of normalised temperature in a range from 0.25-0.65. Even at a relatively low Rayleigh Number of 5.8 $\times 10^5$ non-coherent thermal structures that vary significantly with span and time are seen in the upper portion of the domain near the outer cylinder.

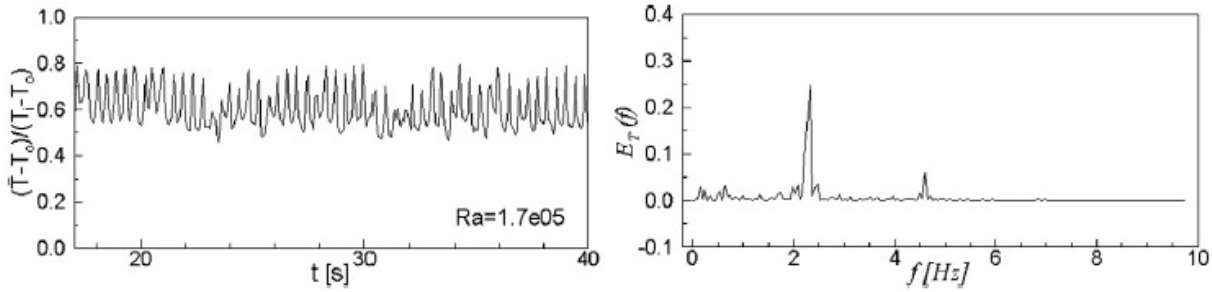

Figure 2.11: Time Resolved Temperature at Mid-Gap $\phi = 0$ and Subsequent Energy Spectra. Adapted [reprinted] from "Large-eddy simulation of transition to turbulence in natural convection in a horizontral annular cavity" by E. L. Padilla and A. Silvira-Neto, 2008, International Journal of Heat and Mass Transfer, 51, 3656-3668, 2008 by Elsevier Ltd.

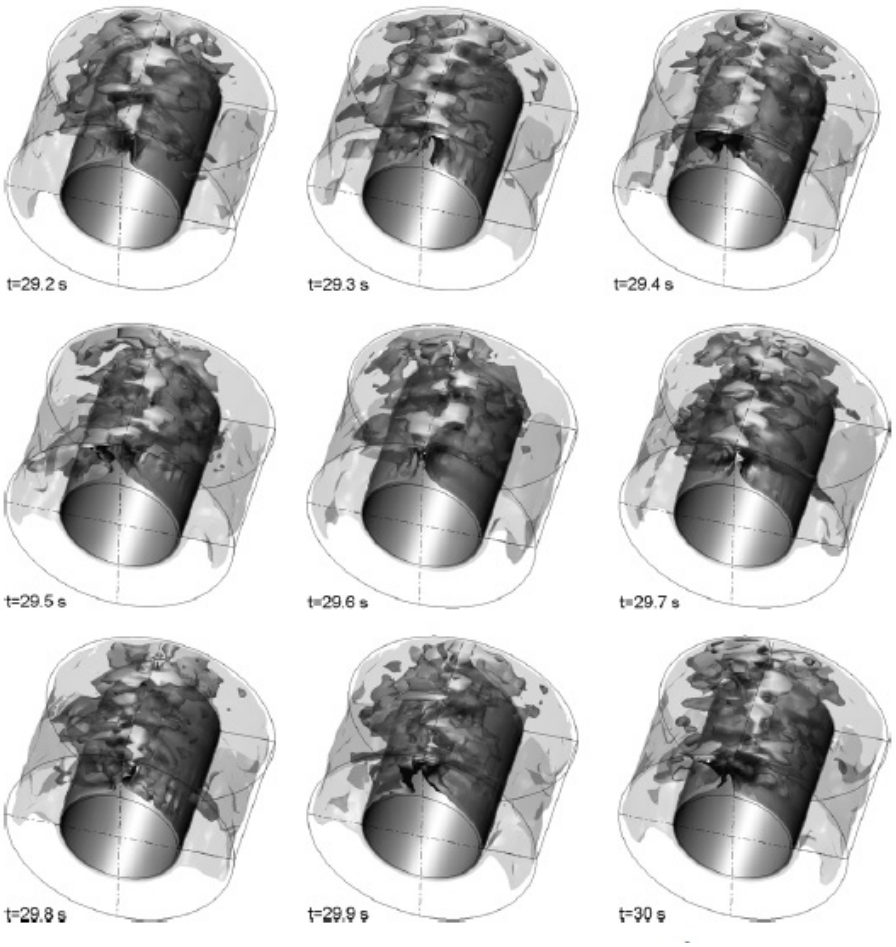

Figure 2.12: Spatial and Temporal Development of Non-Dimensionalised Temperature at $Ra = 5 \times 10^5$. Adapted [reprinted] from "Large-eddy simulation of transition to turbulence in natural convection in a horizontral annular cavity" by E. L. Padilla and A. Silvira-Neto, 2008, International Journal of Heat and Mass Transfer, 51, 3656-3668, 2008 by Elsevier Ltd.

More recently Fadl, He, Stein, and Marinescu (2017) compared 3 time-stepping methodologies to assess the unsteadiness of natural convection with conjugate heat transfer at $Ra = 2.67 \times 10^7$. By modelling the flow with a traditional direct methodology, a loosely-coupled dual-time formulation and pseudo-transient methodologies an assessment of the temporal resolution and accuracy requirements were made. Fadl et al. (2017) found sizeable reductions in runtime (32-40 times)utilising their proposed dual-stepping formulation in comparison to the direct method due to lack of stability restrictions on CFL. Focusing particularly on transient processes, i.e. a linear reduction in inner wall temperature, they investigated changes in physical timestep for the baseline solver in Fluent. Divergence was found at greater timestep sizes than 0.2s.

After initialising from a previous steady-state solution Fadl et al. (2017) compare solutions at t=10s, 160s during the cooling process and find both (dual-time and direct) methodologies are in good agreement with each other (Figure 2.13). They then go onto describe the implications of ramp rate (of inner wall cooling) on the quasi-steady solution with a significant deviation in outer wall heat flux with a change in the temperature gradient.

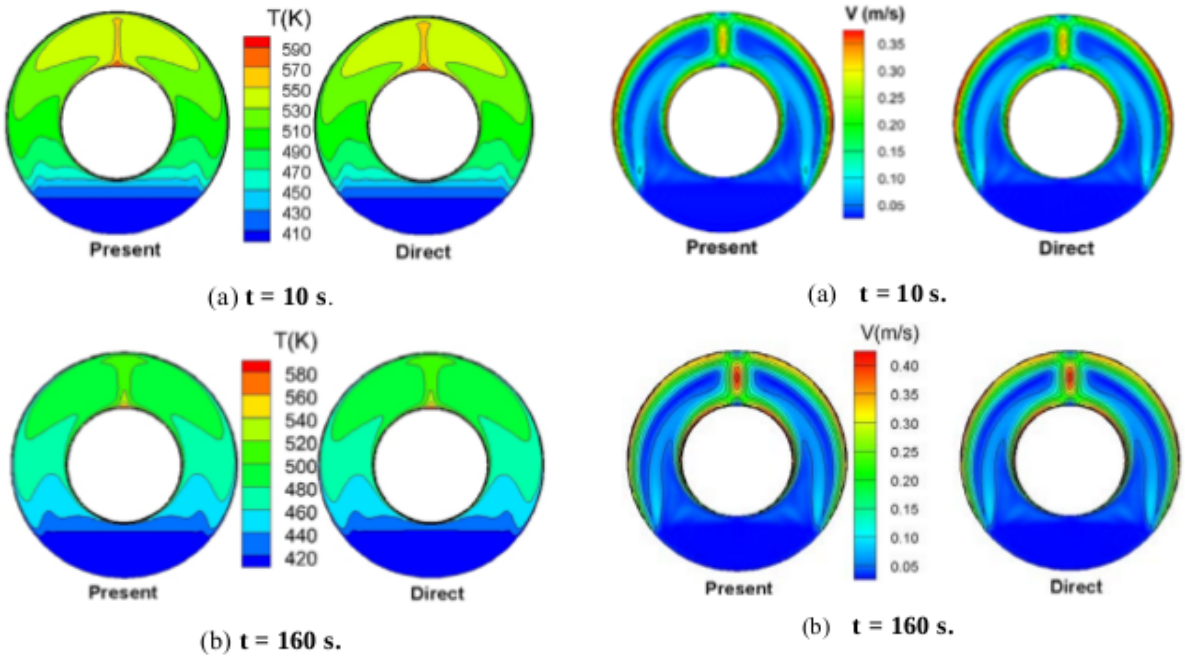

(a) Temperature Contours for Dual-Timestepped ($\Delta t = 10s$) and Direct ($\Delta t = 0.2s$)

(b) Velocity Contours for Dual-Timestepped ($\Delta t = 10s$) and Direct ($\Delta t = 0.2s$)

Figure 2.13: Comparison of Transient Methodologies. Adapted [reprinted] from "Assessment of Unsteadiness Modelling for Transient Natural Convection" by M. Fadl, L. He, P. Stein and G. Marinescu, 2017, Turbomachinery Techincal Conference and Exposition, 26-30/06/2017, Charlotte, NC, USA. American Society of Mechanical Engineers, 2017 by American Society of Mechanical Engineers.

It is important to note here that using a RANS methodology, Fadl et al. (2017) reached a steady-state solution before instigating transient phenomena by changing the inner wall temperature. No evidence of plume migration or meandering has been seen through presented

contours. This contrasts previous literature as demonstrated by Kuehn and Goldstein (1978) and Padilla and Silvira-Neto (2008) who both show the chaotic behaviour of the plume above $Ra \approx 10^5$. It is demonstrated that a transient solution may hold some computational benefits if CFL stability conditions are not a concern (Fadl et al., 2017).

A singular study exists investigating relevant mixed convection studies (Char & Hsu, 1998). Significantly, they present a case with inner cylinder rotation only for $10^4 < Ra < 10^9$ and $0 < Re < 10^5$ for a fluid with a $Pr = 0.7$. Figure 2.14 shows the effect of the rotation of the domain. Char and Hsu (1998) present the dimensionless term Reynolds Number. In this context Reynolds Number is of the form:

$$Re = \frac{R_i \omega L}{\nu} \tag{2.5}$$

At lower Reynolds Numbers up to 10^3, the effect is minor. The thermal plume moves in the direction of rotation, and consequently the location of plume impingement, but convection is still dominant. In case (c), the plume has moved significantly in the direction of rotation and isotherms have started to significantly elongate. Finally, at a Reynolds Number of 10^5 the plume completely breaks down into concentric isotherms and streamlines (Figure 2.14). The authors also present a variation in Ra for constant $Re = 10^4$. Predictably, buoyant phenomena become more dominant with increasing Ra; at a $Ra = 10^7$ a near-constant Nu distribution exists on the outer cylinder, consistent with the concentric isotherms presented in Figure 2.14. With increasing Ra the Nu peak becomes more prominent suggesting a larger influence of buoyant phenomena.

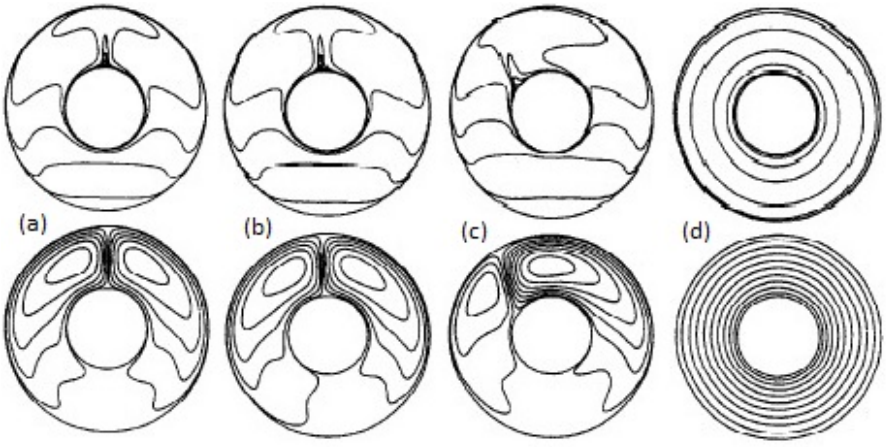

Figure 2.14: Isotherms (top) and Streamlines (bottom) for $Ra = 10^9$: (a) Re = 0; (b) $Re = 10^3$; (c) $Re = 10^4$; (d) $Re = 10^5$. Adapted [reprinted] from "Numerical prediction of turbulent mixed convection in a concentric horizontal rotating annulus with low-Re two-equation models" by M. I. Char and Y. H. Hsu, 1998, International Journal of Heat and Mass Transfer, 110 (12), 1633-1643. 1998 by Elsevier Ltd.

However, tyres exhibit whole domain rotation in contrast to only the inner cylinder in the case of (Char & Hsu, 1998). The presence of concentric rings for both isotherms and streamlines at

lower Reynolds Numbers than the range that is expected, steady state conditions are expected to be achievable.

2.5 Summary

The presented literature review outlines and explains the problem of resolving temperature within a pneumatic tyre and the current literature surrounding natural convection with respect to a Formula 1 context.

The majority of the literature review presented is with respect to natural convection (i.e. $Re = 0$). Both numerical (Francis et al., 2002; Padilla & Silvira-Neto, 2008) and empirical (Bishop, 1988; Kuehn & Goldstein, 1978) studies have been reviewed at up to Ra = 10^9. Studies, presenting data from a variety of perspectives through local Nu distributions to local equivalent thermal conductivity values. The methodologies presented throughout has been discussed at some length, focusing particularly on the numerical studies as they add greater perspective to the intended work.

Kuehn and Goldstein (1978) and Padilla and Silvira-Neto (2008) found plume meandering and chaotic behaviour in the upper part of the domain at (relatively small) Rayleigh Numbers (10^5). LES spectra have shown 2 dominant frequencies in temperature characteristics despite chaotic velocity fluctuation. In contrast, at higher Ra RANS methodologies found steady-state solutions or no plume meandering was witnessed even with a variation in Rayleigh Number or inner wall temperature (Fadl et al., 2017).

Whilst Padilla and Silvira-Neto (2008) demonstrates variation in flow structures both spatially and temporally at fairly insubstantial Rayleigh Numbers, the flow field inside a wheel may markedly differ due to the non-significant implication of whole domain rotation at high Reynolds Number. Char and Hsu (1998) show concentric ring isotherms with inner cylinder rotation only (Figure 2.14), suggesting that a steady state solution is achievable. If this is the case higher-order methodologies would be over-excessive. Additionally, whilst no mention is made to either the computational resource requirements or an explicit time-step value (other than Courant-Friedrichs-Lewy Condition=0.25), Padilla and Silvira-Neto (2008) does state that for LES a refined grid and a small-timestep are required.

All of this contrasts strongly with the case inside a tyre in a motorsport application. High Ra flows are expected (i.e. in the range of 10^7) with significant whole domain rotation with Re (based on mid-radius) in the order of 10^6. Apart from the one mixed convection case (Char & Hsu, 1998) no cited study demonstrated the implication of domain rotation. Even then, Char and Hsu (1998) presented a study with only inner cylinder rotation in comparison to whole

domain rotation. Consequently, a large variance in flow field phenomena is expected from what is currently available in literature.

The bulk of the simulations found presented 2D simplifications with or without symmetrical boundary conditions. Later studies observe significant three-dimensionality of the flow field at lower aspect ratios (Padilla & Silvira-Neto, 2008) thus an extension to 3D study is needed. Whilst the same study also observed a transient flow field at a fairly modest Ra, the implication is unknown for whole domain rotation.

Chapter 3

Methodology

3.1 Geometry

A simplified geometry i.e. a concentric annulus is created to be consistent with the 2018 Formula 1 regulations: front and rear tyre both have dimensions of R_o=335mm with R_i = 6.5" or 165.1mm. The front tyre only is investigated with a width of 305mm (Formula 1 World Championship Limited (2018)). The geometry utilised for this study has dimensions 335 x 165.1 x 302.5 mm (Ro, Ri, w) with an aspect ratio of $\lambda = 1.780$ (3.1).

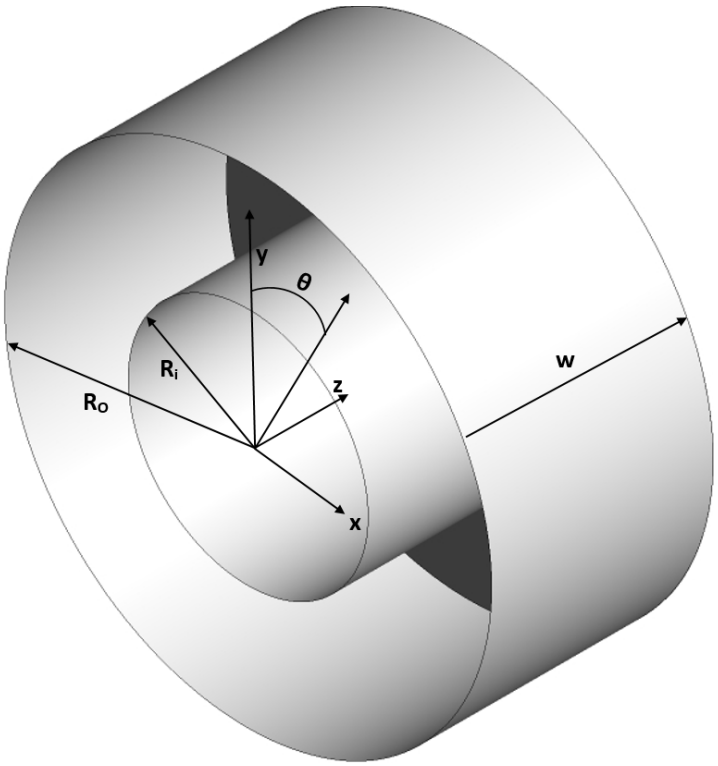

Figure 3.1: Schematic of the Numerical Domain

3.2 Governing Equations

This thesis utilises the Finite Volume technique to solve the compressible Navier-Stokes equations for fluid motion. The equations of motion are reconstructions of the Conservation of Mass (Continuity Equation), Conservation of Momentum (Momentum Equations) and the Conservation of Energy (Energy Equation) Laws. The commercial solver Fluent is used for solution of discretised equations hereout. The equations are presented as follows with the assumption of a compressible, Newtonian Fluid.

Firstly, the Continuity Equation is presented as:

$$\frac{\partial \rho}{\partial t} + \nabla \cdot (\rho \mathbf{u}) = 0 \tag{3.1}$$

With: ρ representing density (kg/m^3) and $\mathbf{u}$ representing the velocity vector (m/s).

The following equation presents the Conservation of Momentum equation for a compressible fluid in notated form:

$$\frac{\partial (\rho u_i)}{\partial t} + \frac{\partial}{\partial x_j}[\rho u_i u_j] = \frac{\partial \sigma_{ij}}{\partial x_j} + \rho g_i \tag{3.2}$$

Finally, the Energy Equation is written as:

$$\frac{\partial (\rho c_p T)}{\partial t} + \nabla \cdot (\rho c_p T \mathbf{u}) = \nabla \cdot k \nabla T + H \tag{3.3}$$

If one examines real-time flow data, it is easy to see large fluctuations in velocity and pressure with time due to the turbulent cascade. Large eddies transfer momentum to smaller scale eddies which eventually dissipate through shear at the Kolmogorov scales. These eddies promote large computational difficulties and do not always present the user with any additional information that is required. Consequently, a technique called Reynolds or ensemble averaging is presented. The velocity and pressure are presented as a function of mean and fluctuating components, i.e.:

$$U = \overline{u} + u' \qquad\qquad p = \overline{p} + p' \tag{3.4}$$

Where:

U : Velocity (m/s)

$\overline{u}$: Mean component of Velocity (m/s)

u' : Fluctuating component of Velocity (m/s)

When applied to the Navier-Stokes Equations, and by noting that the mean of the fluctuating component, $\overline{u'} = 0$; a non-linear term appears on the right-hand side of the momentum equation of the form:

$$\tau_{ij} = -\rho\overline{u_i' u_j'} \tag{3.5}$$

Known as the Reynolds Stress tensor, this term is symmetrical meaning that only 6 unknowns have been introduced. A technique known as the Bousinessq Hypothesis is presented which is essential to the majority of the work within this thesis. The hypothesis relates the Reynolds stress term to a product of the mean stress and a newly introduced term, the turbulent viscosity (μ_t). This technique assumes isotropic stresses which in the case of strong recirculating or separated regions is not the case.

$$\tau_{ij} = 2\mu_t S_{ij}^* - \frac{2}{3}\rho k \delta ij \tag{3.6}$$

Where:

μ_t : is the Turbulent Viscosity

S_{ij}^* : is the Mean Strain Rate Tensor.

k : is Turbulent Kinetic Energy

δ_{ij} : is the Kronecker Delta.

k is defined as the root mean squared of velocity fluctuations i.e.:

$$k = \frac{1}{2}(\overline{u'u'} + \overline{v'v'} + \overline{w'w'}) \tag{3.7}$$

3.3 Turbulence Modelling

3.3.1 K-ϵ

Formulated and proposed in its current form by Launder and Spalding (1974), the model is a 2 equation, semi-empirical, eddy viscosity model. It proposes transport equations for the above mentioned, turbulent kinetic energy (k), and its rate of dissipation (ϵ). K-ϵ has been utilised successfully for convection in horizontal cylinder annuli by Char and Hsu (1998).

3.3.2 RNG K-ϵ

More critically to this study, RNG-k-ϵ is a variation on the model proposed by Launder and Spalding (1974). This variation formulated by Yakhot and Orzag (1986) derives additional

terms in the epsilon equation and a modified effective viscosity that improve accuracy, particularly in strained flow fields better predicting production and dissipation of turbulent properties (Tu, Yeoh, & Liu, 2013; Versteeg & Malalasekera, 2007). Francis et al. (2002) showed that RNG-k-ϵ is a suitable approach to modelling natural-convection and as such will be utilised in the mixed convection case presented along with the Kato production limiters utilised by Char and Hsu (1998).

3.4 Boundary Layer Modelling

The overwhelming majority of the published work regarding natural convection uses a Low Reynolds Number formulation utilised for wall-modelling (Char and Hsu (1998); Francis et al. (2002)). Consequently, Low-Reynolds Number wall models will be utilised in the rest of this body of work. "Enhanced Wall Treatment" is utilised, that through the use of a blending function, combines the 2-layer formulation Jongen (1992) and single layer formulation of (Fluent Inc. (2006); Wolfstein (1969)). If dimensionless wall-distances (y^+) is sufficiently fine the blending function weights the 2-layer formulation more significantly. As $y^+ < 1$ criterion is set on first-layer height values for this work; the use of Enhanced Wall Treatment will be similar to the previous studies i.e. Francis et al. (2002), Tu et al. (2013).

3.5 Numerical Methodology

The Finite-Volume Method (FVM) is utilised for the discretisation of transport equations onto discrete cells. This technique utilised by a number of commercial codes, breaks up a larger control volume into a number of finite discrete cells or elements. The RANS equations are then disctretised onto cell centres in integral form, i.e. a volume integral is taken of the transport equations over each cell. Using a combination of discretisation and interpolation schemes over neighbouring cells, an iterative approach is used to ascertain an approximate final solution (Tu et al., 2013). They further explain, the benefits of FVM stating that due to the nature of the scheme, FVM can utilise a wider range of cell types including structured and non-structured grid types.

3.5.1 Discretisation Schemes

Schemes that interpolate face values from cell-centres are needed for a number of terms in the RANS equations, most critically the convective terms in any transport equation (Versteeg & Malalasekera, 2007). For convective terms in the momentum equation, the total variation diminishing scheme (TVD) Monotonic Upwind Scheme for Conservation Laws or MUSCL scheme is selected. First implemented by Van Leer (1979) TVD schemes address the oscillation

that can occur in certain residuals with larger ratios of convection to conduction (Peclet Number) (Versteeg & Malalasekera, 2007). This is achieved by artificially weighting the upstream contribution.

Turbulence properties are discretised with upwind schemes as has had success in Francis et al. (2002). Upwind schemes are utilised with high-Peclet numbers as central-differencing does not demonstrate transportiveness (Versteeg & Malalasekera, 2007). However, upwind schemes suffer from false-diffusion with non-aligned faces to flow direction.

Like Francis et al. (2002), the Body-Force Weighted scheme for pressure interpolation is utilised. This scheme, similar in nature to Rhie and Chow (1983) interpolation uses a colocated grid whereby pressure and velocity are stored at cell-centres and interpolated to face values. This for natural convection is advantageous as the impact of the non-zero pressure gradient, due to buoyant body force term, at the boundary is taken into account (Fluent Inc., 2006). This scheme is particularly useful when the body force term is known *a priori* and is constant.

3.5.2 Pressure-Velocity Coupling

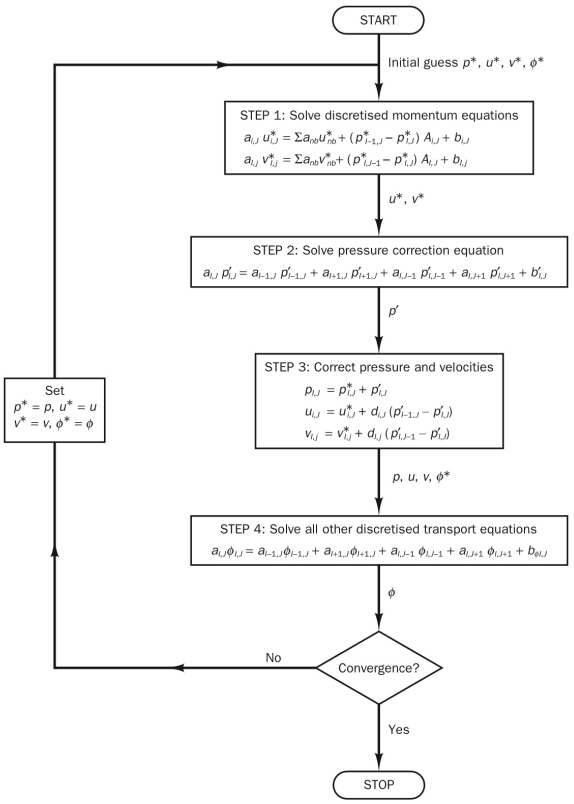

Figure 3.2: Block Diagram of the SIMPLE Pressure-Velocity Coupling. Adapted [reprinted] from "Computational Fluid Dynamics: A Practical Approach" by J. Tu, G. H. Yeoh, and C. Liu, 2013, Butterworth-Heinemann, Waltham, MA, USA. 2013 by Butterworth-Heinemann.

An iterative approach is used to solve the discretised Navier-Stokes equations mentioned previously. The method proposed by Patankar and Spalding (1972) known as Semi-Implicit Method for Pressure-Linked Equations or *SIMPLE* for short, is used throughout. This methodology utilising a "guess and correct" approach as discussed in Tu et al. (2013). Initial guesses are taken for pressure and velocity from which the momentum equations are solved. A pressure-correction equation is then solved, from which updated momentum and pressure equations are then solved. Finally, these values are used to solve for other transported properties such as turbulent kinetic energy, dissipation and further as an initial guess for the next iteration. Figure 3.2 demonstrates this procedure visually using a block diagram.

3.6 Transient Formulation

For the presented transient results the First-Order Implicit transient formulation is utilised. Fluent Implicit time-stepping uses a dual-time formulation in which an additional pseudo-time derivative, $\frac{\partial}{\partial \tau}$, is introduced to a given transport equation. Through additional iterations at each individual time-step the pseudo-time derivative is forced to zero, replicating the original transport equation (Fluent Inc., 2006). This equation now takes the form of:

$$\frac{\partial}{\partial t}\int_V W dV + \Gamma \frac{\partial}{\partial \tau}\int_V Q dv + \oint [F - G] \cdot dA = \int_V H dV \tag{3.8}$$

Both pseudo and real-time derivatives are then discretised by a first-order backward difference scheme (which is not presented here; for further details see Fluent Inc. (2006)). It is important to note that this formulation is not conditionally stable based on the Courant Number (CFL), $(\frac{u\Delta t}{\Delta x})$ and thus the timestep is only constrained by the desired level of temporal resolution (Fluent Inc., 2006). Thus CFL ≤ 40 was set as a target.

3.7 Initial Conditions

Turbulence Properties are set with respect to the following formulae, set iteratively by utilising peak velocity magnitude from previous simulations on coarser grids (CFDOnline, 2014). In the case of high-Ra flows an estimate of 0.15m/s was used, with a turbulence intensity of 10%.

$$k = \frac{3}{2}(UI)^2 \qquad \epsilon = C_\mu \frac{k^{\frac{3}{2}}}{l}$$

$$l = 0.038(R_{outer} - R_{inner}) \tag{3.9}$$

3.8 Thermophysical Properties

Some conjecture within literature exists with respect to a methodology to calculate reference temperature at higher Rayleigh Numbers. Francis et al. (2002) utilises an arithmetic-mean temperature for the appraisal of fluid properties; Char and Hsu (1998) utilise a two-thirds volume weighted average towards the inner boundary. Transport properties will vary with temperature, and at higher Rayleigh numbers these values can deviate significantly from one end of the temperature range to the other. For this work the arithmetic mean will be used:

$$T_{ref} = \frac{T_{higher} + T_{lower}}{2} \tag{3.10}$$

Temperature boundary conditions(Table 3.1) are set at:

Temperature	
Patch Id	Temperature (° C)
T_{inner}	200
T_{outer}	100
Top and Bottom	Adiabatic

Table 3.1: Temperature Boundary Conditions

From here the thermophysical properties are evaluated as previously suggested at the arithmetic mean through the use of Wischnewski (2018) and all case setups are presented as an Appendix A.

Density is calculated through the use of the ideal-gas law. Similar to Francis et al. (2002) the compressibility factor was found through use of Wischnewski (2018) at p=23psi and T_{ref}= 423.15K and was found to be 1.00. Thus, minimal deviation from ideal-gas is seen and the ideal-gas assumption will be sufficient. Fluent Inc. (2006) calculates density via:

$$\rho = \frac{p_{op} + p}{\frac{R}{M_w}T} \tag{3.11}$$

With p_{op} representing the user-specified operating pressure, p, the local relative pressure and R and M_w representing the universal gas constant and gas molecular weight respectively. Additionally, for these simulations, a polynomial variation of C_p and constant transport properties were used i.e. constant μ and Pr.

3.9 Rotational Boundary Conditions

The whole domain is set with moving wall boundary conditions as well as frame motion. Fluent sets this by determining and setting the tangential velocity at cell centre on the boundaries. Further information can be found in Fluent Inc. (2006). In this case, rotation can be considered 2D and thus boundary conditions are set using the formula:

$$v = \omega \times r \tag{3.12}$$

Fluent Inc. (2006) however, calculates tangential velocity in a 3D manner where ω and r are vectors representing the angular velocity and radius respectively. The rotation axis must therefore be defined being the z-axis. Angular velocities are set using estimates between the slowest speeds on the Formula 1 calendar (which the author believes would be around 50km/hr at the Fairmont Hairpin in Monaco) to the highest speed (being approximately 360km/hr at the end main straight at Monza, Italy). Boundary conditions for inner, outer cylinders and sidewalls in addition to the entire domain are set with explicit angular velocity calculated by the above equation.

Here the non-dimensional Reynolds Number is presented as a function of the arithmetic mean of rotational velocities i.e:

$$\begin{aligned} U =& (\frac{R_o + R_i}{2})\omega \\ Re =& \frac{UL}{\nu} \end{aligned} \tag{3.13}$$

3.10 Solution Procedure

Convergence criteria for all residuals except energy have been placed at 10^{-3}. Energy convergence criteria has been set at 10^{-6}. All final solutions are achieved by the gradual ramping of the gravity vector using consecutive converged steady-state simulations. Four ramps in the gravity vector were required from 0.0981, 0.981, 2 and finally to 4.5. This reduces the magnitude of the body-forces and allows the flow to sufficiently develop before advancing the solution. Any ramp in the gravity vector greater (for natural convection simulations) than 4.5 with $\Delta T = 100K$ and $p_{gauge} = 23psi$ produced an oscillating solution with continuity residual greater than 10^{-3} and as such were not considered. This is possibly due to the significant non-linearities associated with natural convection.

Additionally, significant under-relaxation is required to reduce the magnitude of solution oscillation. Under-relaxation factors of 0.01-0.1 for all flow variables except energy are utilised based on the case Rayleigh Number. Energy under-relaxation factors are set at or close to 1.

With these under-relaxation factors, a significant number of iterations are required to achieve convergence. Most simulations required 30,000 plus iterations to converge. Consequently, a solution similar to multi-grid (where a method called prolongation is used to achieve faster convergence) is utilised to check mesh independence. Convergence is achieved on the base grid before interpolating that solution data onto finer grids as the initialisation condition. This reduces subsequent iterations on the finer grids significantly and hence speeds up convergence.

3.11 Verification and Validation

3.11.1 Mesh Generation

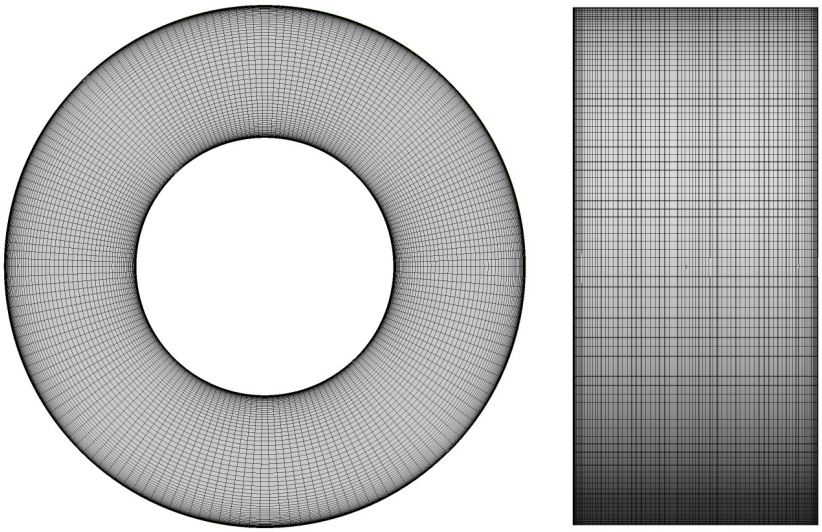

Figure 3.3: Medium Structured Mesh

A first-order structured grid approach is used in this scenario. Figure 3.3 visualises the medium mesh employed for the following grid-refinement study. Uniform spacing is utilised for the angular grid distribution, whilst a hyperbolic distribution is chosen for both radial and spanwise directions in order to adequately resolve both velocity and thermal boundary layers.

3.11.2 Grid Refinement Study

Table 3.2 shows the results for the 3 structured grids employed for the grid refinement study. The grid independence check was performed at a constant Rayleigh Number of Ra = 5.020 $\times 10^6$ and Re=0. Percentage change was found via Nusselt Number at $\theta = 0$ at the spanwise mid-plane and Nusselt Number distribution at the same plane is shown in Figure 3.4. Minimal variation (i.e. 0.475%) between the Medium and the Fine meshes was seen in peak Nusselt

Number and minimal variation over the angular distribution with an additional 38% of cells, thus the mesh is considered adequate.

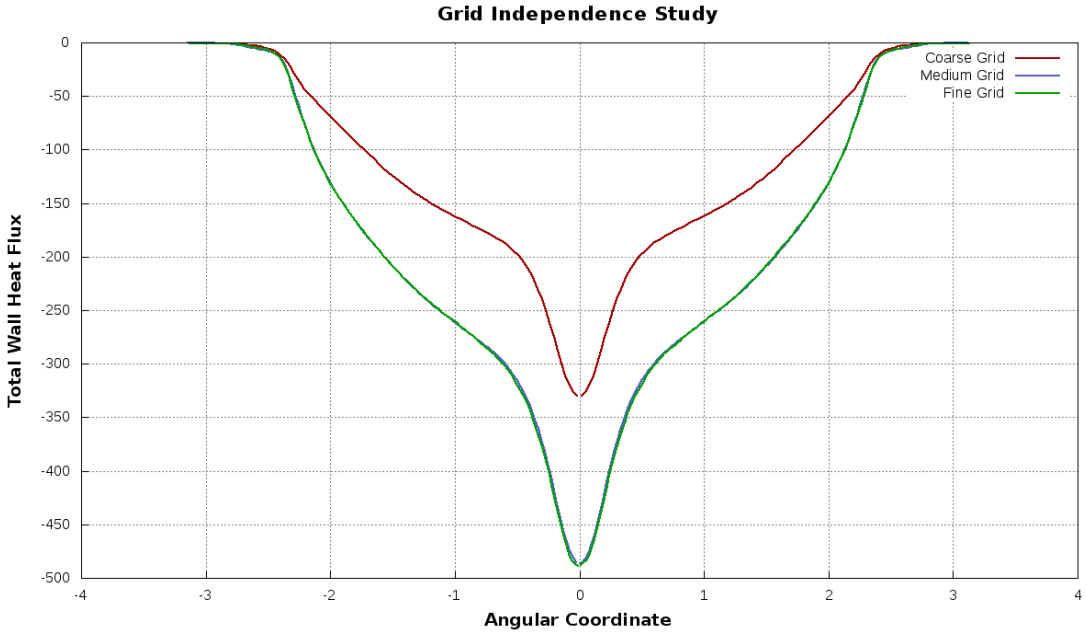

Figure 3.4: Grid Refinement Study

Grid Refinement Study			
Grid Name	Grid Cell Distribution	Cell Count	Percentage Change
Coarse	179 x 80 x 81	1,124,960	32.535
Medium	249x130x151	4,798,800	0.475
Fine	299x150x176	7,770,350	N/A

Table 3.2: Grid Refinement Study

3.11.3 Validation

Validation has been performed against Kuehn and Goldstein (1978) at $Ra = 2.51 \times 10^6$ and with nitrogen as the working fluid. A 2D geometry with symmetry is created shown in Figure 3.5. The domain represents a 2D section of Kuehn and Goldstein (1978) experimental setup with R_o and R_i set at 0.0462m and 0.0172m respectively. Francis et al. (2002) validates similarly and presents physical properties as follows: internal pressure values are set at 3,500kPa with inner and outer-wall temps set at 28.1 and 27.2 ° C respectively. By taking a volumetric average thermal conductivity is set at 0.02735 (W/m-K) and specific heat at 1141.4 (J/kg-K). Finally, Prandtl Number is set at 0.731, kinematic viscosity at 4.462×10^{-7} and a density at 39.3 (kg/m^3).

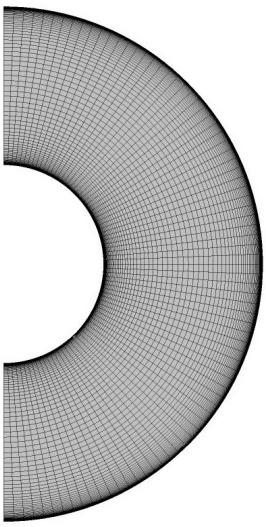

Figure 3.5: Computational Domain showing Mesh Lines

As Figure 3.6 (left) shows, and similar to Francis et al. (2002), the methodology presented shows acceptable agreement with Kuehn and Goldstein (1978). All temperature distribution show correct distribution shapes, however, the thermal plume somewhat over predicts (by roughly 10%) the normalised temperature profiles. Numerous wall-modelling options and production limiters were tested to try to address this issue, however, none had a drastic impact and the best result is presented. Outside the plume, an acceptable quantitative agreement is shown between current methodology and the empirical studies.

Figure 3.6 (right) shows a qualitative reperesentation of the flow field coloured by temperature with red and blue colouring representing areas of higher and lower relative temperatures respectively. The figure also demonstrates the angular position of the interrogated temperature profiles shown in Figure 3.6.

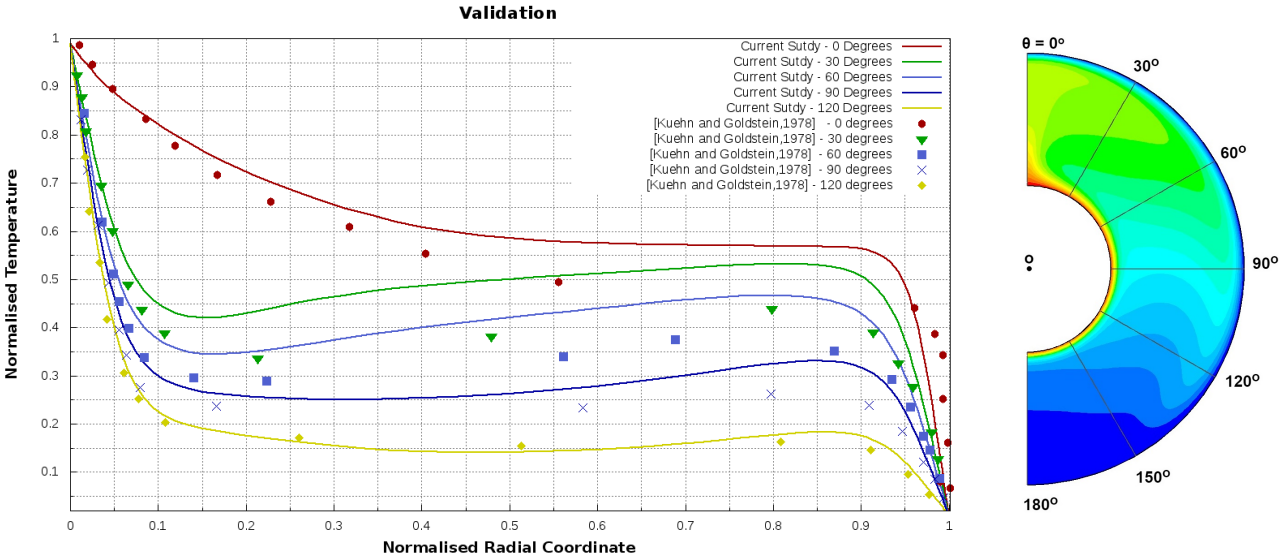

Figure 3.6: Normalised Temperature at Varying Angular Position vs Kuehn and Goldstein (1978)

Prior works also over-predict the temperature profiles in the bulk fluid (Char & Hsu, 1998; Desai & Vafai, 1994; Francis et al., 2002). The impression and the distinction that Francis et al. (2002) made, however, that correlation within the bulk-fluid (i.e. outside the boundary layer) improved with increasing Rayleigh Number. Consequently, the methodology was deemed acceptable.

3.12 Computational Requirements

As simulations performed are of significant mesh density and require a large number of iterations, computations were performed on the HPC cluster Raijin managed and maintained by National Computational Infrastructure (NCI). Each node at NCI is installed with 2x 8 core Intel Xeon E5-2670 "SandyBridge" processors equipped with 32,64 or 128GB of DDR3 memory. Jobs were submitted using either 32 or 64 cores and ranged from 4-48 hours for 30,000 iterations depending on the mesh density. All runs were post-processed on a local machine.

A number of simulations were also performed on an Amazon Web Service (AWS) m4.16xlarge instance with 64 Intel Xeon E5-2686 v4 CPU with 256GB DDR4 memory. Simulations on this architecture took roughly 16 hours for 20,000 iterations on a 5-million element mesh.

Chapter 4

Results

4.1 Steady-State Natural Convection

Results are first evaluated for an annulus at a $Ra = 5.020 \times 10^6$ undergoing natural convection ($Re = 0$), a simplified representation of a tyre sitting stationary on the grid or during a pitstop. Other implications such as the change in shape and the thermal source at the contact patch could cause variations in flow structures, however, the implication is dependent on the relationship between track temperature and ambient and is difficult to generalise without introducing additional variables and a significant amount of complexity outside the scope of this thesis.

As per reviewed literature, a thermal plume exists at $\theta \approx 0$. The plume forms and rises through buoyant forces and impinges on the outer cylinder and then falls along the outer cylinder wall in an attached buoyant jet. Two counter-rotating vortices form above the inner cylinder shown in Figure 4.1, tending to dominate and drive the flow in the upper section of the domain. Further, thermal and velocity boundary layers form on the inner cylinder due to heated positively buoyant flow near the wall rising. Outside the outer cylinder buoyant jet in the upper section of the cylinder (i.e. $\theta < 120°$), the flow tends to deviate significantly and rise back towards the plume. Beyond $\theta \approx 90°$ a local area of negative buoyancy shows flow direction change and fall downwards towards the inner cylinder boundary layer. Finally, an almost stagnant region exists in the bottom section of the annulus ($\theta > 120°$), where the value of buoyant body forces is at a minimum.

In conjunction with a stagnation point, a local recirculation region exists at $\theta \approx 0$ on the inner cylinder. Due to the buoyant forces, the inner cylinder boundary layer separates locally at the base of the plume. In-plane streamlines show this clearly (Figure 4.2) detailing also how this phenomena varies along the length of the cylinder. In Figures 4.2a and 4.2b the recirculation region seems to be less significant, however, closer to the middle of the cylinder (i.e. Figures

4.2c and 4.2d) this recirculation region seems to be fairly prominent.

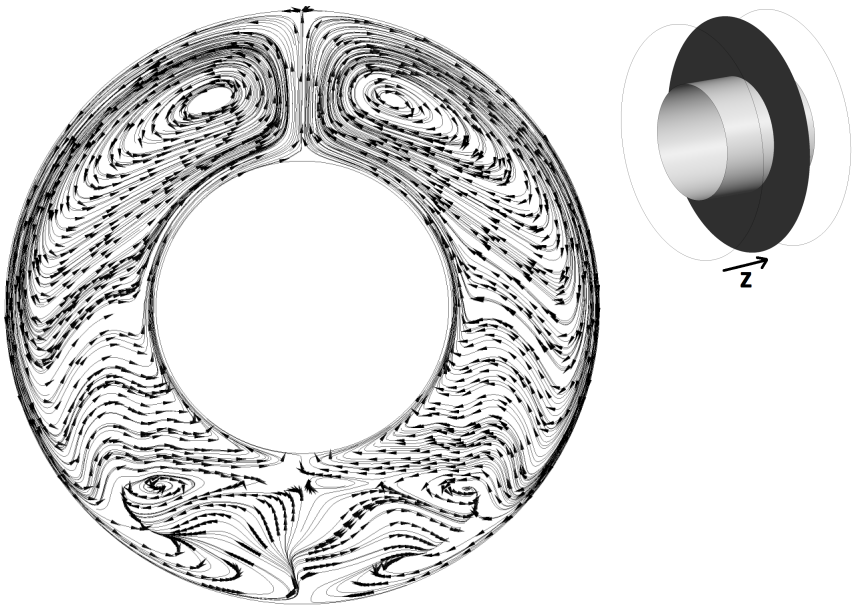

Figure 4.1: In-Plane Velocity Streamlines at z = $\frac{7w}{15}$

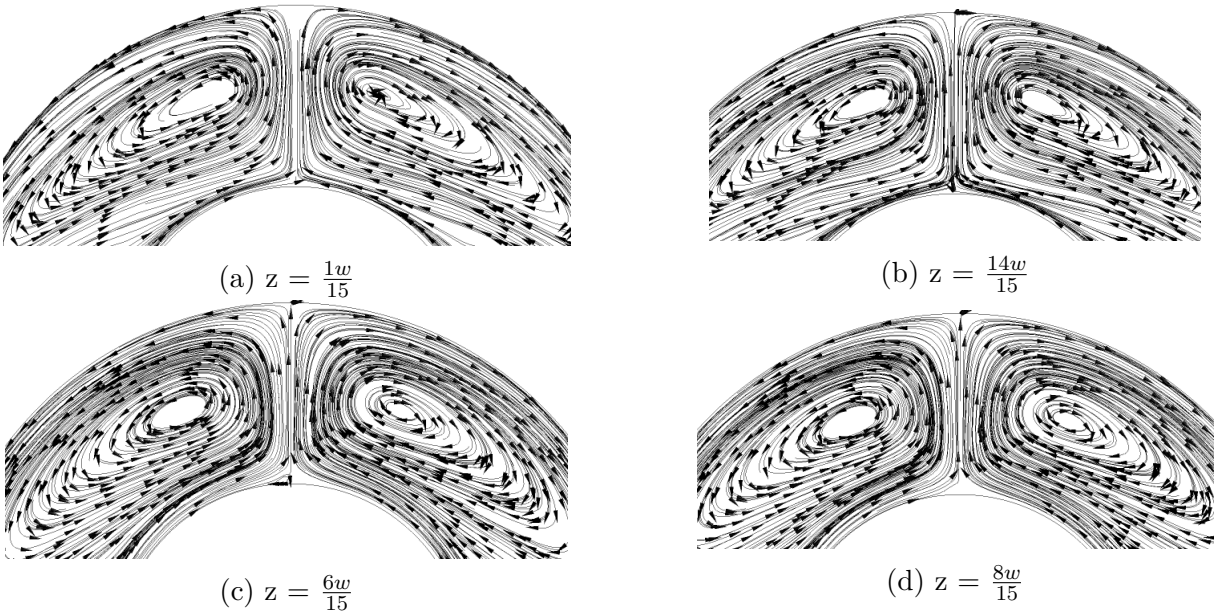

(a) z = $\frac{1w}{15}$ (b) z = $\frac{14w}{15}$

(c) z = $\frac{6w}{15}$ (d) z = $\frac{8w}{15}$

Figure 4.2: Spanwise Normalised Temperature Contours

The 2 prominent vortices also vary significantly between the 4 locations presented in Figure 4.2. Closer to the insulated walls the vortices tend to migrate upwards closer towards the centre of the annulus above the inner cylinder. The movement of the vortices is most likely the main factor behind variation in the local recirculation region and upper inner cylinder stagnation point.

As the flow is driven by buoyancy, regions with the largest velocity magnitude are expected in locations with the most significant thermal gradients, i.e. around the inner cylinder, the plume and the buoyant jet along the outer cylinder. Figure 4.3 shows this clearly with contours of velocity magnitude: a region of high-velocity flow exists in the region of $10 < \theta < 45°$, created by the upper domain vortices.

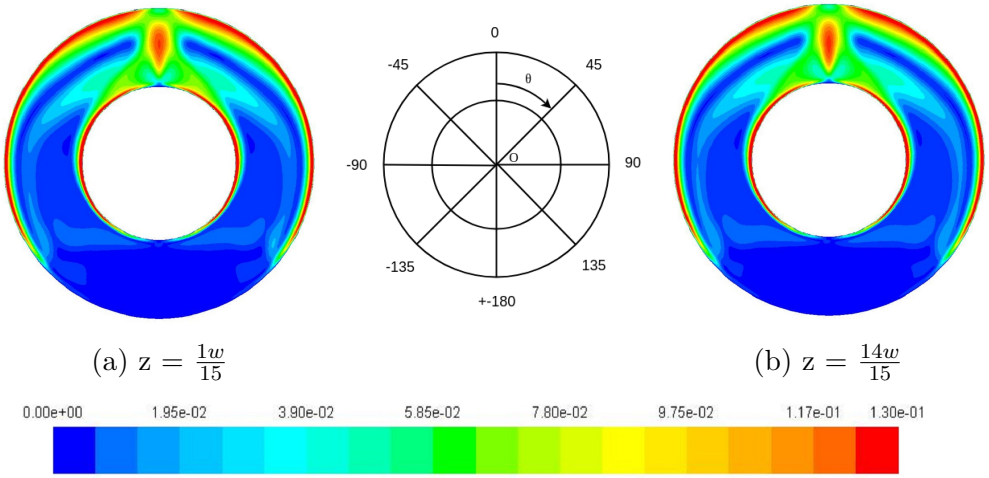

(a) z = $\frac{1w}{15}$ (b) z = $\frac{14w}{15}$

Figure 4.3: Velocity Magnitude (m/s) Contours

By comparing Figure 4.3 with Figure 4.4 stark differences in flow structures are seen. The additional velocity region outside the inner cylinder shear layer and the buoyant jet in Figure 4.4 is notably less discernible. The plume, however, seems to be more distinguishable with higher velocity values within this region. A stagnation point is now also clearly seen in the impingement region on the outer cylinder at $\theta = 0$. This would indicate that some out of plane motion exists near the impingement region in Figure 4.3.

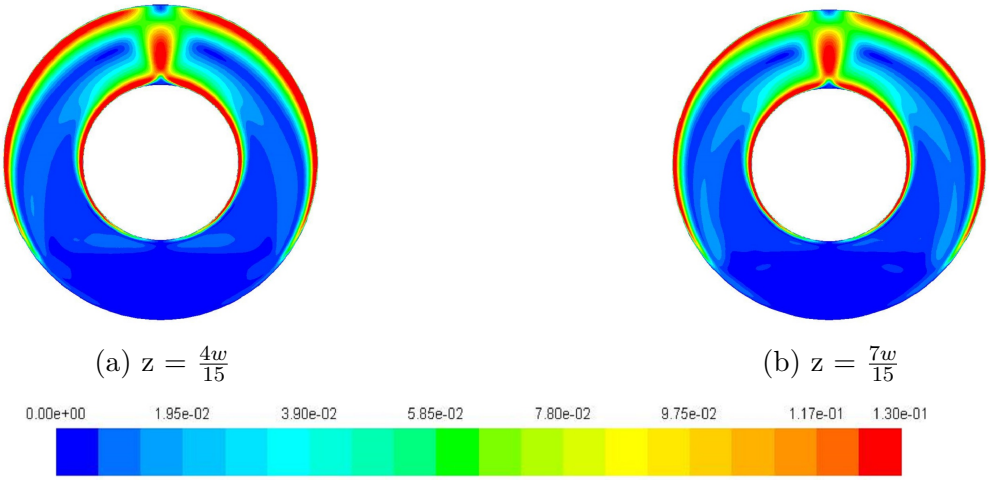

(a) z = $\frac{4w}{15}$ (b) z = $\frac{7w}{15}$

Figure 4.4: Velocity Magnitude (m/s) Contours

The formation of 2 counter-rotating vortices in the upper corners of the domain in the cross-section of the thermal plume is shown in Figure 4.5. This behaviour explains the results seen

previously in Figure 4.3. Away from the sidewall 2 symmetrical regions of out of plane behaviour (z-velocity) exists with significant 3-dimensionality occurring in the impingement region in the end thirds of the domain. Closer to the inner cylinder larger regions of lower z-velocity occur showing axisymmetric properties. Finally, cellular formation is inhibited due to positive buoyancy in the majority of the upper domain; instead, the middle third of the span exhibits minimal out of plane motion.

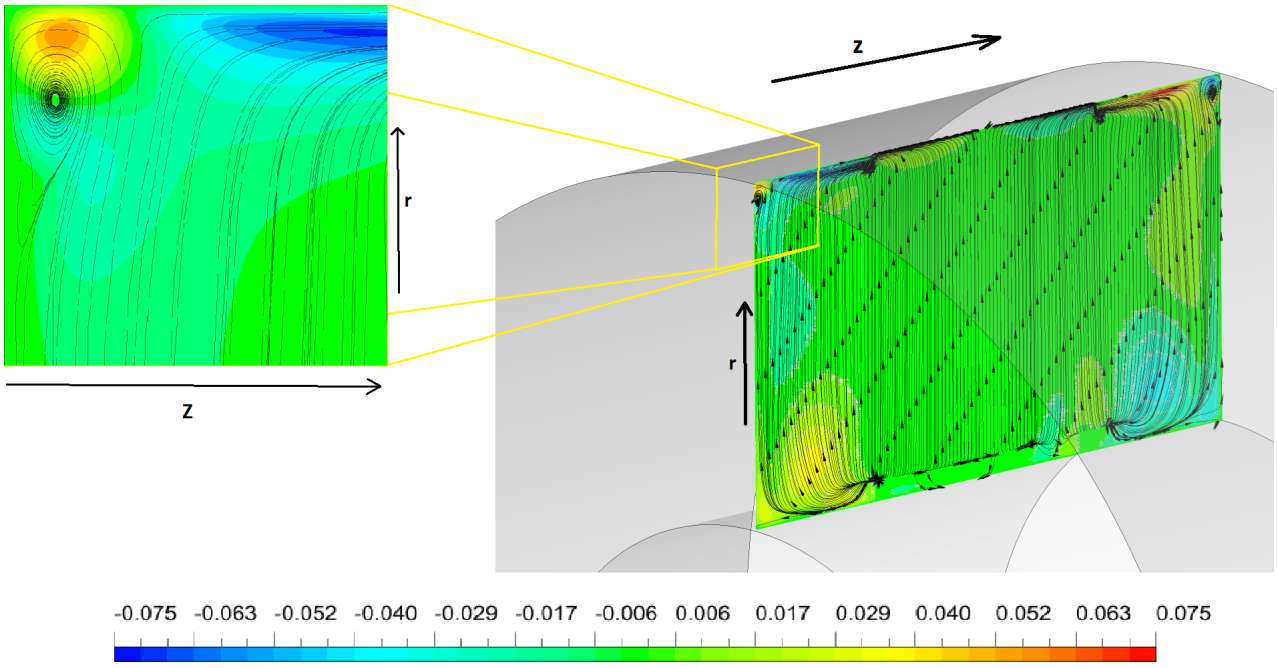

Figure 4.5: Surface Streamline and Vz Contour (m/s) at $\theta = 0$

Figure 4.6 demonstrates the variation in normalised temperature and the variance in significant thermal structures over the span of the domain. On the adiabatic wall the lower thermal resistivity causes the plume to dominate the upper portion of the domain (Figure 4.6-(a)) in comparison to the planes closer to the mid-span (Figure 4.6-(b-c)). The plume does not however seem to be consistent along the length of the domain with Figure 4.6 (d) showing a much thinner plume than both the centre of the domain and close to the adiabatic sidewall.

Consistent with previous literature presented in this *Ra* range turbulent production and dissipation is limited to the upper half of the domain and more significantly where both buoyant and shear forces are dominant i.e. the plume and inner and outer wall shear layers. With turbulent production only limited to these regions, the results tend to indicate that only part of the domain is turbulent consistent with results presented by Farouk and Güçeri (1982). Further, these properties do vary over the span, even close to the mid-plane with the buoyant jet almost tending to thin and elongate closer to the mid-plane.

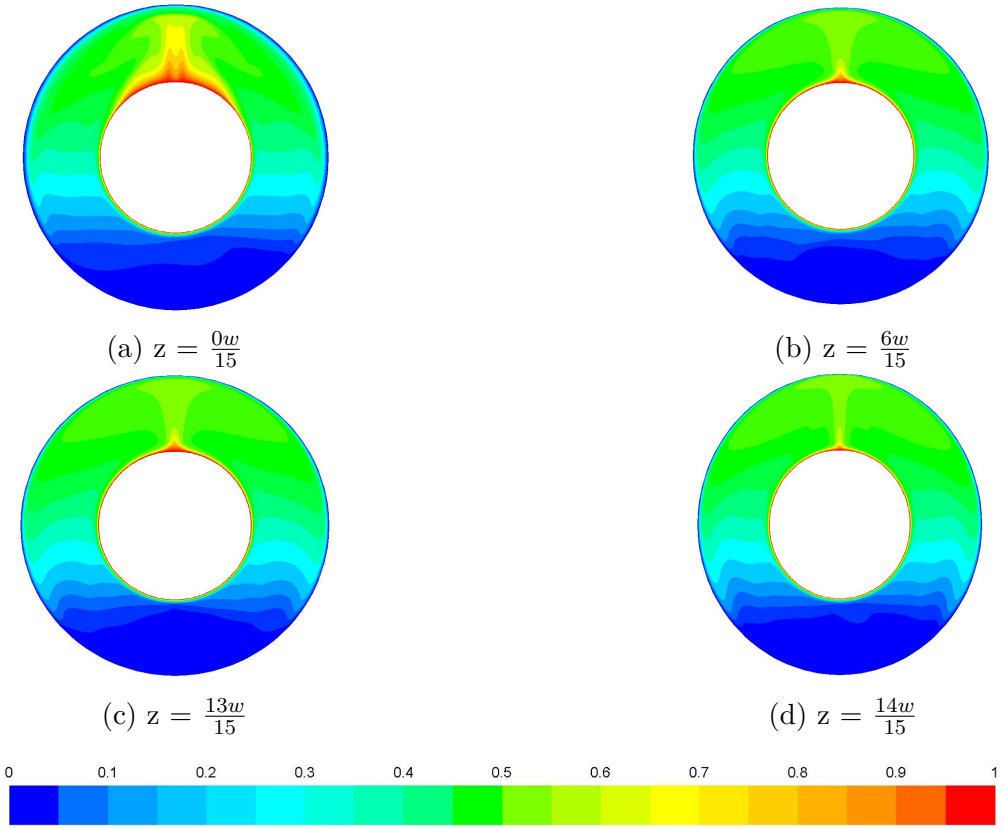

(a) z = $\frac{0w}{15}$ (b) z = $\frac{6w}{15}$

(c) z = $\frac{13w}{15}$ (d) z = $\frac{14w}{15}$

Figure 4.6: Spanwise Normalised Temperature Contours

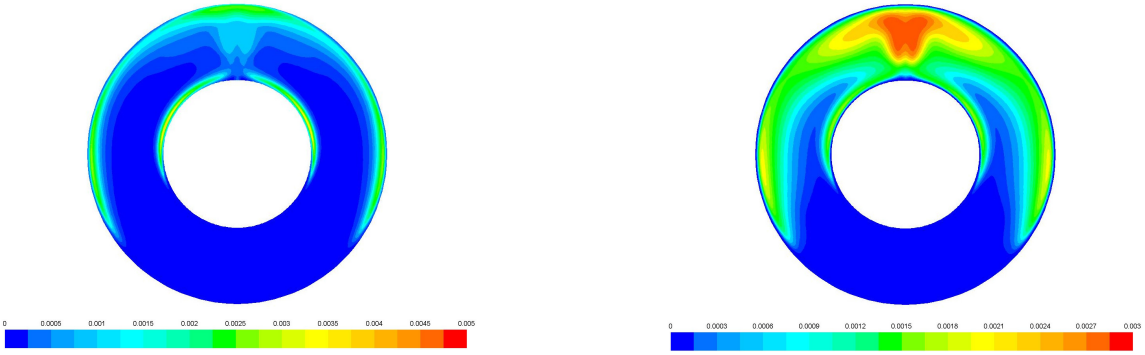

(a) ϵ (m^2/s^3) (b) k (m^2/s^2)

Figure 4.7: Turbulence Properties at the Mid-Plane

Similar properties are seen in the outer cylinder heat transfer with Figure 4.8 presenting a 3D surface of outer-cylinder Nusselt Number coloured by value. As expected with normalised temperature plots, the lower thermal resistivity near the adiabatic walls seems to significantly enhance the local Nusselt Number values. Further, between roughly $0.3w - 0.6w$ (i.e. $0.1 < z < 0.2$) an almost constant Nusselt Number core can be witnessed with only minor variation in both shape and peak value over the middle third of the domain. However, what is more obvious and significant from the 3D surface, is the appearance of a region with significantly higher thermal resistivity, where the impingement is almost completely degraded and peak Nusselt Number occurs away from $\theta = 0$. These regions (between $0.05 < z < 0.1$ and

$0.2 < z < 0.25$) almost appear symmetrical lengthwise. This behaviour is possibly explained by the implications of the 3D impingement and significant out of plane velocity near the outer cylinder in these regions in particular.

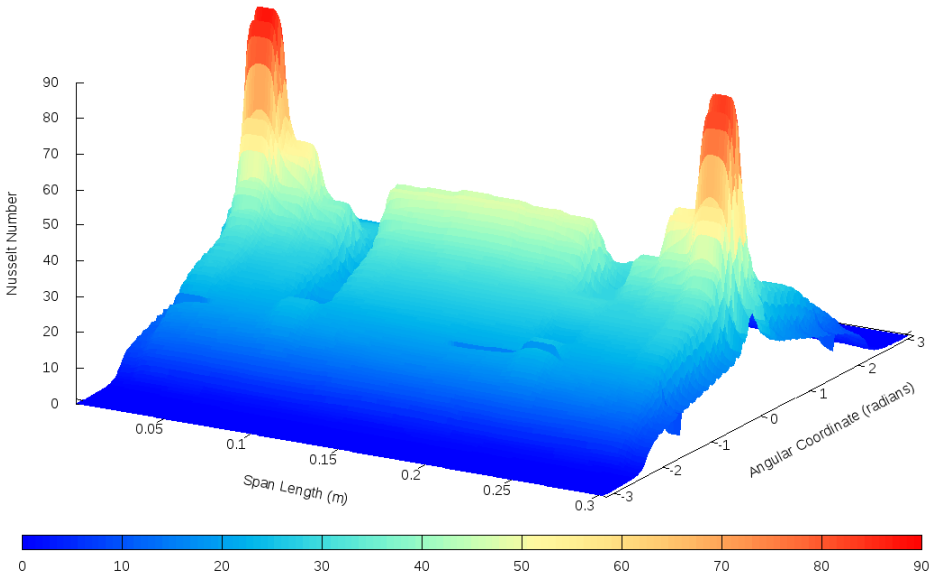

Figure 4.8: 3D Surface of Outer Cylinder Nusselt Number

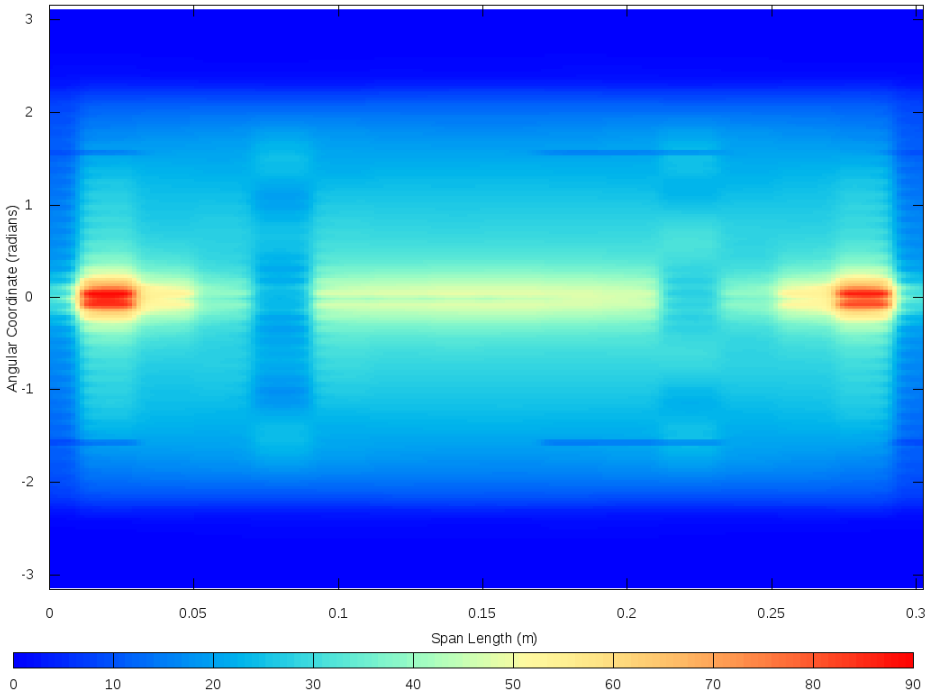

Figure 4.9: Outer Cylinder Nusselt Number Contour

The 3D surface is quasi-symmetric about the mid-z and mid-x planes showing differences mainly in peak Nusselt Number values in the spike near the adiabatic walls. This is shown better by

a plan view in Figure 4.9 which is a plan (top) view of the 3D surface presented in Figure 4.8. Non-symmetric effects are also seen in the more diffuse regions with $0.2 < z < 0.25$ showing a less diffuse nature than $0.05 < z < 0.1$. With the Nusselt Number peak at $z = 0$ slightly larger than the other end it is possible that the more diffuse or higher thermal resistivity in the diffuse region is directly linked to the behaviour at the side wall. However, particularly in the middle third of the domain (i.e. $0.1 < z < 0.2$ or the "core") minimal variation in both peak Nusselt Number value and location can be seen, suggesting for this span thermal effects are quite homogenous.

4.2 Transient Natural Convection

Transient simulations were also performed at the same Ra for performance and flow comparisons. The flow was resolved with $\Delta t = 0.01s$ for a total of 45s of real time. Time histories (from 25-45s) of temperature and velocity variations in the plume on the spanwise midplane (locations are shown in Figure 4.10) are presented in Figure 4.11a and 4.11b respectively.

After initial fluctuation for a period of roughly 20s, both temperature and velocity fluctuations tend to damp out and reach quasi-steady-state solutions with no significant or dominant frequency of oscillation. The time history shows a period of 20s in which temperature only varies by approximately 0.1 degree or 0.05% and velocity decrease by 0.02 m/s or roughly 1.8%. Such little fluctuation is considered inconsequential and could be due to fluctuation in residual histories. With velocity and temperature fluctuations being inverse in this circumstance and the buoyant body force being the driving influence behind flow within the domain, significant variations are not expected with larger time interrogations.

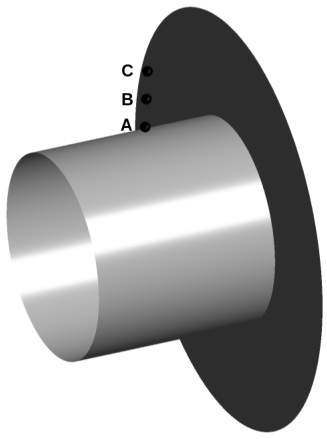

Figure 4.10: Point Locations

Point Locations			
Point	X	Y	Z
A	0	0.2	0.15125
B	0	0.25	0.15125
C	0	0.30	0.15125

Table 4.1: Point Locations

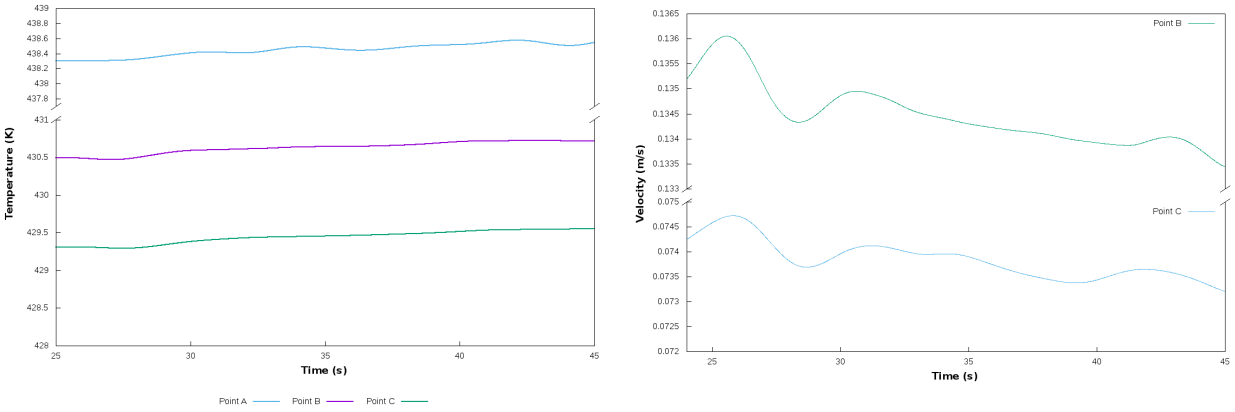

(a) Temperature

(b) Velocity Magnitude

Figure 4.11: Time Histories

Similarly, outside the plume, normalised temperature shows minimal variance or deviation between t = 38.5s or t = 44.8s. Figure 4.12 demonstrates this through a spanwise midplane normalised temperature contour. Shape and size of the plume and outer jet fluctuations are consistent across both suggesting no observable differences in the solution between the two timesteps.

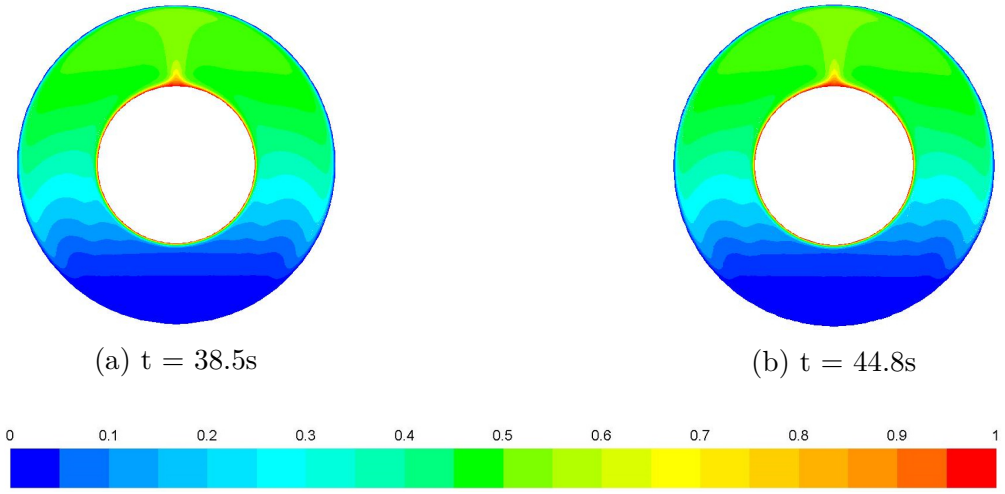

(a) t = 38.5s

(b) t = 44.8s

Figure 4.12: Midplane Normalised Temperature Comparison

Direct comparison between the transient and steady-state solutions offers similar conclusions. As per Figure 4.13, normalised temperature is almost identical between 4.13a and 4.13b with only noticeable deviations occurring at $\theta > 120°$. The steady-state solution in this region tends to slightly degrade or poorly resolve the shape of contours.

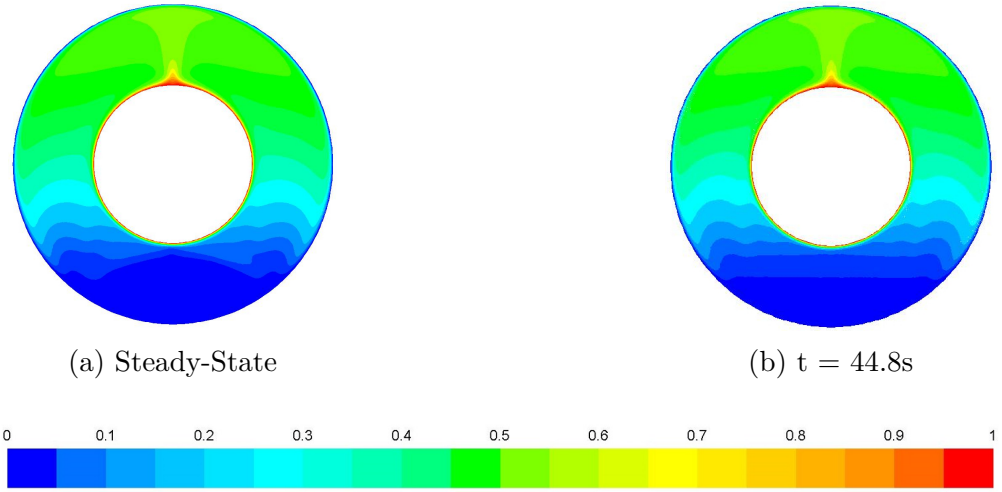

(a) Steady-State (b) t = 44.8s

Figure 4.13: Spanwise Normalised Temperature Contours

Further investigation of normalised temperature in this region ($\theta = 140°$) shows only a 2.5% variation between the steady-state and transient solutions closer to the outer wall. At $0.05 < \frac{R-R_i}{L} < 0.3$ a nearly constant 1% positive offset is seen, Figure 4.14, suggesting an over-prediction of temperature in this region using the steady-state solution. The effect on outer cylinder Nu, however, is expected to be minimal with only a small thermal gradient and an even smaller variation between solutions close to the outer cylinder.

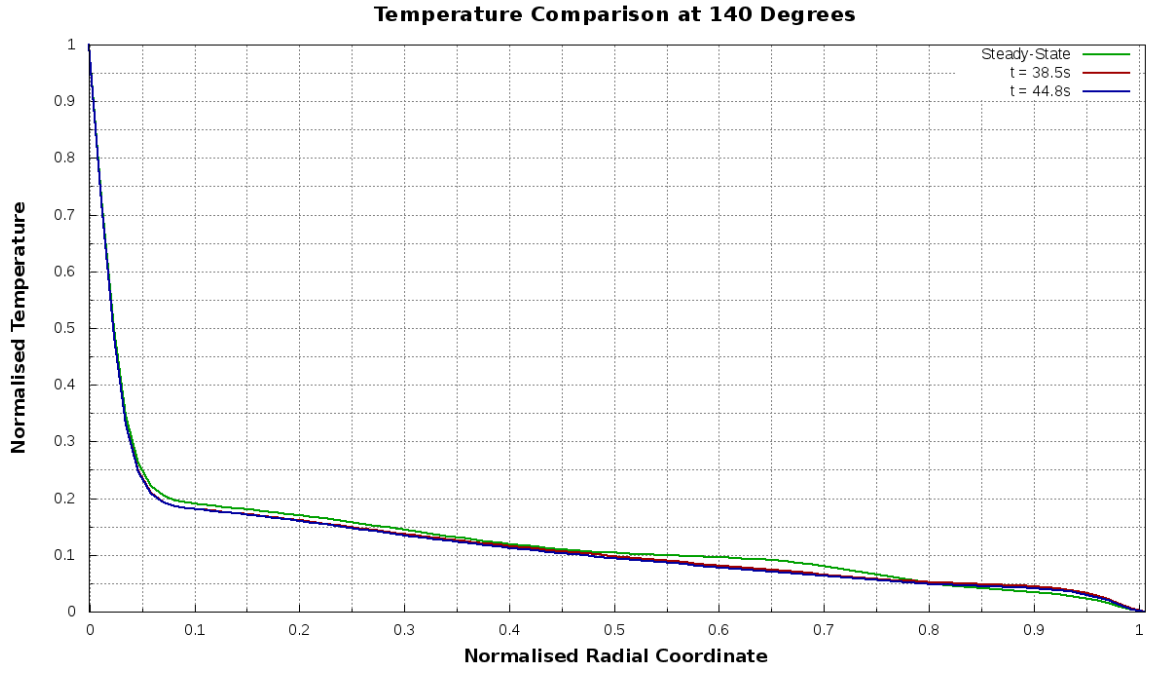

Figure 4.14: Normalised Temperature Comparison at $\theta = 140°$

A direct comparison between all 3 solutions is then made via Figure 4.15. An excellent quantitative agreement is reached between all 3 series, with the steady-state solution only slightly deviating between $0.05 < \frac{R-R_i}{L} < 0.1$ with steady-state solution slightly overpredicting tem-

perature.

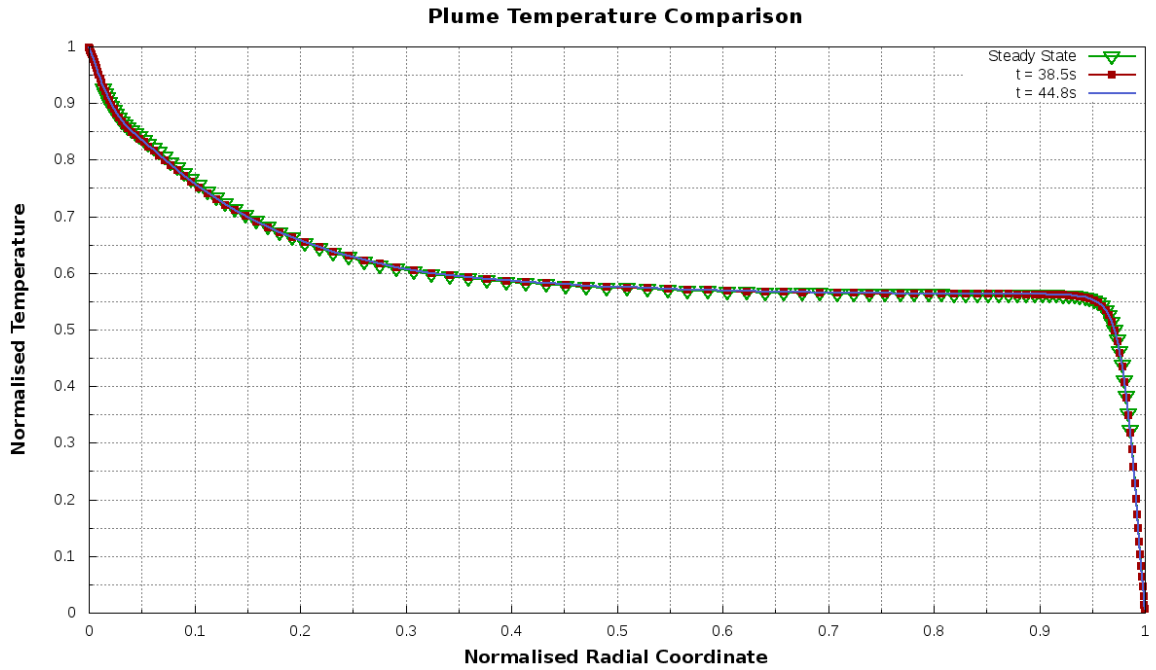

Figure 4.15: Temperature Comparison

Whilst Fadl et al. (2017) only present transient simulations with varying boundary conditions, the results presented are similar qualitatively in terms of no visible chaotic motion of the plume. In contrast, literature was presented that suggested that chaotic motion of the plume existed at Ra $> 10^5$. Both methodologies do not resolve this suggesting that either that small-scale instabilities are the main cause of this phenomenon or large timesteps tend to damp these fluctuations.

Performance statistics and total runtime are then examined for both the steady-state and transient solutions on the same mesh. The steady-state solution reached residual criteria fairly quickly though required roughly 25-30,000 iterations to see a minimal variance in temperature. The transient simulation was rerun for 35,000 iterations with $\Delta t = 0.01$s (i.e 35s). Performance statistics are shown in Table 4.2. On average it took transient simulations less time per iteration to solve the discretised equations, however, each iteration took roughly 0.709% longer, suggesting larger write times over the length of the simulation. Assuming run time scales linearly with iterations, a solution time increase of 17.49% is witnessed for 35s of runtime and 51.06% for 45s vs the comparative steady-state solution.

Performance Comparison			
Run Type	Time solving Linear Equations (s)	Time Per Iteration (s)	Total Time (s)
Steady-State	1.471	2.960	88786.570
Transient	1.442	2.981	104336.842

Table 4.2: Timestepping Performance Comparison

The simulations were run on the same mesh with both runs initialised from a steady-state solution on a coarser mesh. A further decrease in CFL or increase in mesh density are likely not to have any major impact on the solutions temporal accuracy as Fadl et al. (2017) showed agreement with much larger timesteps. Further, the expected dominant frequencies for temperature are between 2-5Hz, as shown by Padilla and Silvira-Neto (2008) and with a solve frequency of 100Hz upwards of 20 points per period should be sufficient for full temporal resolution.

Consequently, the conclusion that both are acceptable alternatives is reached. With only 0.709% time difference per iteration, the number of iterations is the main factor in varying solution time. Further investigation may yield that an increase in timestep and CFL would yield similar results and consequently reduce the number of iterations required for the transient solutions and hence drastically reduce the solution time. Apart from the number of iterations, whilst the transient simulations are faster solving the linear-equations every iteration, time per iteration is increased because of the larger write time. Reduction in the number and frequency of data files written, i.e. one data file, for repeat solutions once transient statistics are known, may reduce solution time even further.

4.3 Effects of Reynolds Number

Effects of Re are investigated at a Ra of 1.094 $\times 10^7$. Re is varied by changing whole domain rotation values. The implications on velocity, temperature and heat transfer phenomena at the outer cylinder are investigated.

The implications on velocity are presented and qualitatively compared against the Natural Convection case discussed previously. Figure 4.16 shows a linear velocity gradient between inner and outer cylinders. This is demonstrated by equispaced concentric rings on the contour plot. This velocity gradient is directly proportional to the product or radial coordinate and angular velocity. No velocity variation near-wall is seen suggesting no presence of a near wall velocity boundary layer. In comparison, advection dominates the flow field with velocity values 2 order of magnitude higher than the $Re = 0$ case. Even with the change in Ra, velocity values 100 times those exhibited in the $Re = 0$ scenario are not expected, suggesting a minimal influence of the buoyant body force.

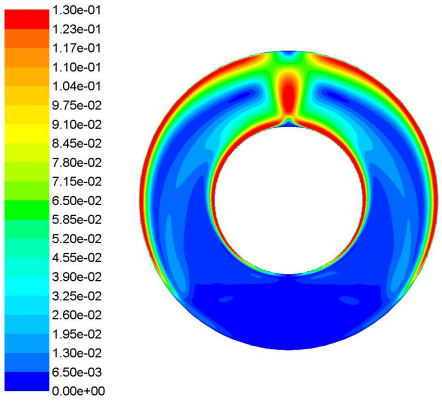

(a) Ra = 5.020 $\times 10^6$, Re = 0

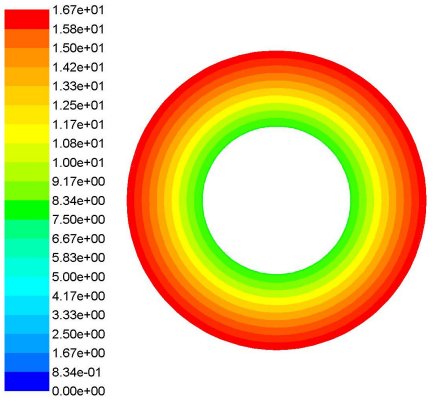

(b) Ra = 1.094 $\times 10^7$, Re = 4.851 $\times 10^5$

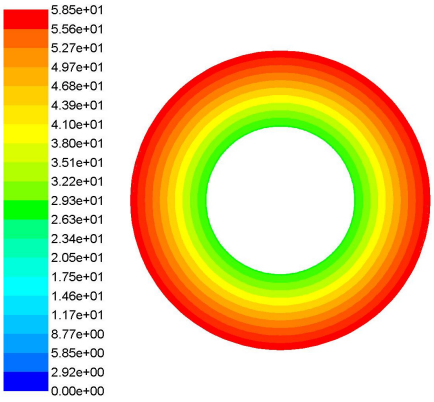

(c) Re = 1.698 $\times 10^6$

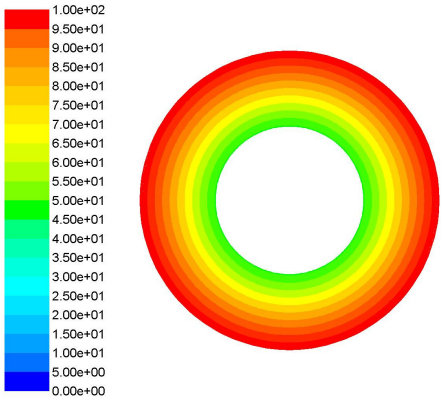

(d) Re = 2.910 $\times 10^6$

Figure 4.16: Velocity Magnitude at z = $\frac{7w}{15}$

Temperature, however, shows minimal variation with increasing Re. All cases exhibit nearly constant normalised temperature values suggesting the implication of rotation is to mix and

diffuse the thermal flux resulting in homogenous temperature and density throughout the domain. Thin thermal boundary layers can be seen near both inner and outer cylinder created by the imposed boundary conditions.

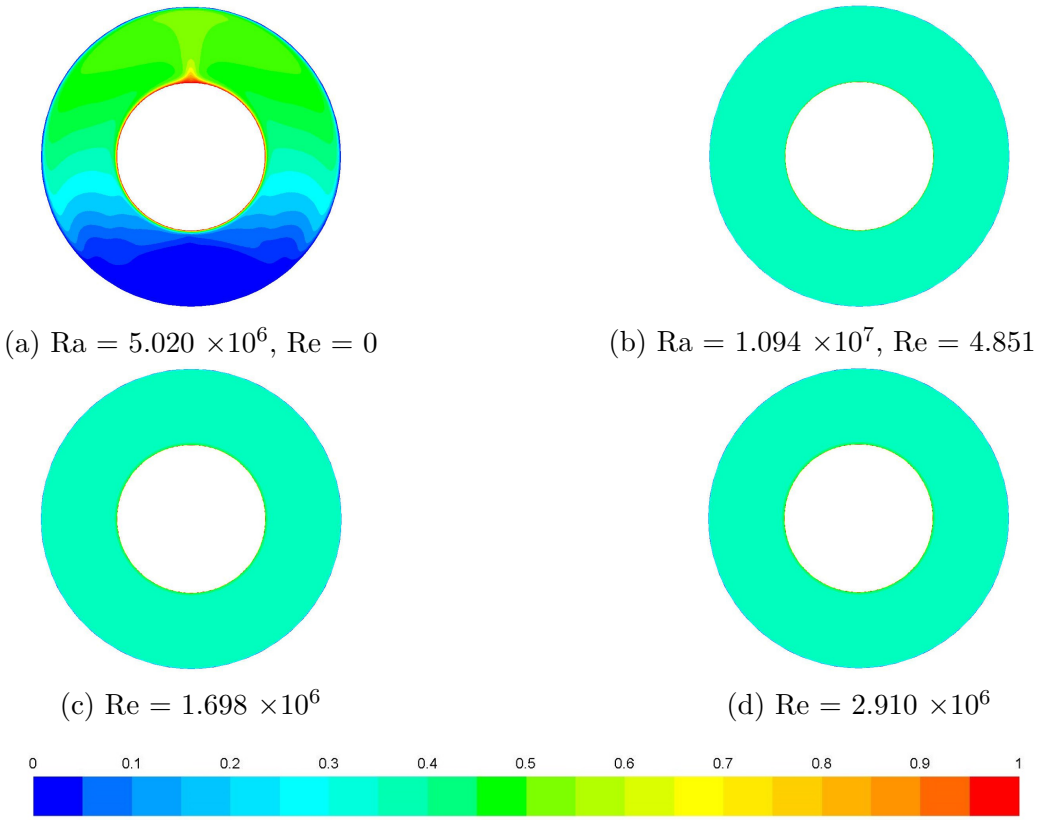

(a) Ra = 5.020 $\times 10^6$, Re = 0

(b) Ra = 1.094 $\times 10^7$, Re = 4.851 $\times 10^5$

(c) Re = 1.698 $\times 10^6$

(d) Re = 2.910 $\times 10^6$

Figure 4.17: Normalised Temperature at z = $\frac{7w}{15}$

The 3D surfaces of outer cylinder Nu in Figure 4.18 show the effects of angular velocity on outer cylinder heat transfer. Only a weak correlation between Re and Nu is observed peak Nu between $Re = 4.851 \times 10^5$, 1.698×10^6 with peak Nu increasing by 19.3% at slower Re with respect to the higher Re case. Between $1.698 \times 10^6 < Re < 2.910 \times 10^6$ Nusselt Number does not show this inverse proportionality and only minimal deviation can be seen between the two cases. In all cases, the 3D surfaces are uniform across all span and angular coordinates again suggesting a minimal implication of buoyant body force on heat transfer phenomena.

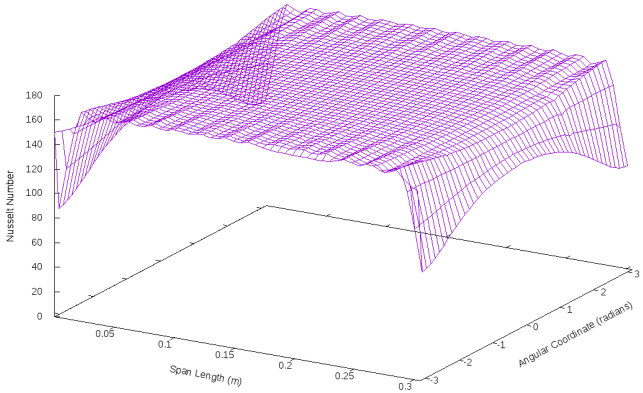

(a) Re = 4.851 $\times 10^5$

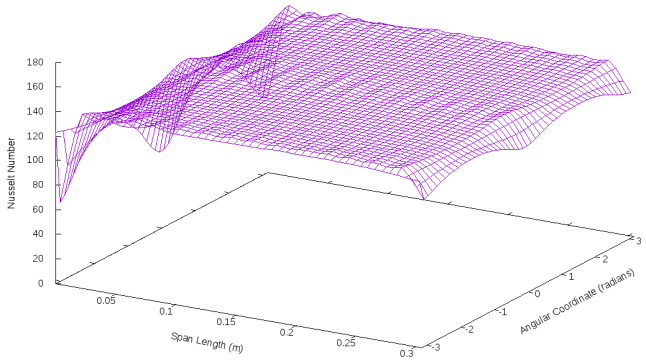

(b) Re = 1.698 $\times 10^6$

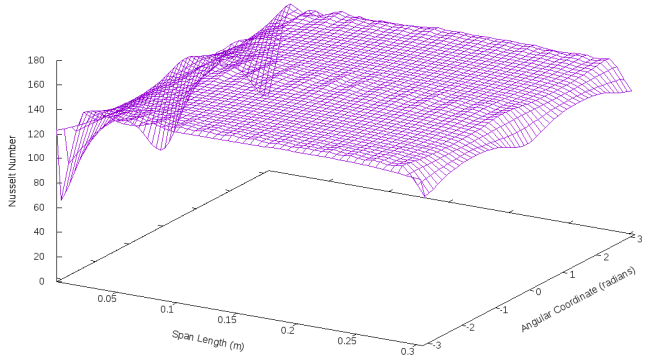

(c) Re = 2.910 $\times 10^6$

Figure 4.18: Nusselt Number Variation over Outer Cylinder with Reynolds Number

Chapter 5

Conclusion

5.1 Discussion

The results and methodologies presented are intended for use as development paths and strategies for controlling thermal dissipation in modern motorsport. The results show a few implications of some of the many variables that affect heat transfer.

Steady-state methodologies were primarily considered due to contextual resource requirements. Steady-State simulations, in general, take substantially less time to reach a solution than transient counterparts and as such with any resource limitations are generally first considered. At higher *Ra* and due to the extreme under-relaxation factors used to prevent residual oscillation, solutions required a significant number of iterations to reach convergence. Further, convergence required a number of gravity vector ramps to reach a final acceptable solution. Perhaps, transient simulations may not need these treatments and thus may not require as significant resource expenditure. In this particular case, they may be worth investigating. Additionally, in such a naturally transient regime resolving total implications of plume meandering on the distribution of heat fluxes and Nusselt number may deserve further consideration.

Whilst URANS or transient simulations were conducted they failed to show the implications of plume meandering on outer-cylinder impingement or the mean temperature and velocity fields as was expected. Possible explanations include: the temporal resolution (i.e. CFL number), the spatial resolution (the grid size) and turbulence modelling. Considering plume fluctuations are chaotic above Ra $=10^5$ it is possible that the length and time scales influencing this effect are not-resolved with current methodologies. Consequently, the implications are two-fold: temporal resolution needs to be increased, i.e. reduction of CFL number to > 1 or spatiotemporal resolutions need be considered.

Considering the first of the two implications; a 40 fold reduction in CFL requires a 40 fold increase in computational time as the two are inversely proportional. With respect to the

time scale of this current work, it was simply outside the bounds and therefore possible to place within the scope. With the suggestion that First-Order Implicit transient formations being non-conditionally stable convergence criteria was the only consideration when picking a timestep and respective CFL, not necessarily the temporal resolution required.

With regards to the second: turbulence cascades from the mean flow and largest length and time scales to the Kolmogorov scales then dissipates through internal shear as heat. Using Eddy-Viscosity models, this cascade is statistically modelled and not resolved. It is possible that the unresolved scales are the driving influence behind plume meandering and as such RANS methods may not resolve this phenomenon. More significant research is needed to suggest whether or not the spatial resolution of the turbulent cascade is required to any significant degree. This would be achieved through higher-order turbulence modelling methodologies such as Stress-Blended Eddy Simulations, Detached Eddy Simulation or Large - Eddy Simulation.

Conversely, it may also be possible to increase the timestep and CFL to reduce the solution time. If meandering is not a consideration and only mean flow is, the increase in CFL may provide a reasonable alternative to steady-state methods at higher Rayleigh Numbers as such significant and aggressive under-relaxation is not needed to reduce any oscillation. Further, a pseudo-transient formulation may also significantly accelerate convergence in comparison to the segregated solvers utilised in this work. If convergence could be achieved using this formulation significant speedup may be achieved.

Prolongation or interpolation from previous steady-state simulations proved to help dramatically with convergence and runtime for both transient and steady-state cases. By initialising with a steady-state solution, the number of iterations per timestep can be reduced drastically and as such total number of iterations greatly reduced.

Considering the methodology to resolve performance statistics: performance statistics were taken with mean data produced at the end of a run. Minimal to no runtime processing with regards to CPU or memory load was considered even though both simulations were run on the same instance. For greater insight runtime processing with respect to CPU, memory and write statistics would be beneficial.

Other modelling techniques such as the Boussinesq approximation have shown promise in reducing solution oscillations and increasing stability. These methodologies were not considered in this case due to the significant temperature difference between the inner and outer walls giving rise to large thermal property variations.

With regards to the current methodology, simplifications were introduced that may have a

sizeable impact on flow features and thermal phenomena. The simplifications were introduced to reduce both the number of variables and the scope in light of the time-scale of the current work. Convection, either natural, mixed and forced, is influenced by a number of surface properties for instance surface roughness that were not considered that may be avenues for further research. Further as previously mentioned, the geometrical and thermal simplifications may have implications on the results. Track and ambient conditions vary significantly over a season and for example, the ambient, track and the difference between the ambient and track temperature, at Barcelona, Spain in winter testing will not be the same as Monza, Italy in the summer. These relationships are significant and conjugate studies including radiative and conduction effects may show differences to what is presented in the current work.

Finally, thermal sources in the tyre are inherently transient and non-homogeneous however here have been presented as steady and homogeneous over surfaces. The contact patch through adhesion is a significant source of tyre temperature, and both the radiative and conductive effects from the rim vary significantly even through a braking phase. As this data was not accessible, approximations had to be made.

5.2 Recommendations for Future Work

This thesis presents mixed convection data for a simplified tyre geometry at a range of both Ra Re. Recommendations based on the results are presented for areas of future investigation that could hold some value.

In noting limitations in the current computational procedure, both temporally and spatially resolved methodologies would allow for investigations to cover a much larger array of Ra. Padilla and Silvira-Neto (2008) has conducted some of this work at transitional Ra, however, this could be extended to gap widths, radius and aspect ratios similar to a tyre. With the plume being inherently unsteady (most likely due to small scale instabilities), spatially and temporally resolving the flow field would give greater insight into the overall implications of the flow-phenomena. This would be conducted through scale-resolved methodologies i.e. Implicit LES.

The geometry presented is a significant simplification of the tyre itself. The rim is generally a one-piece magnesium construction with the geometry close to the tyre bead becoming inherently more complex. Such geometry may have implications on the flow field particularly around the bead which has a large implication on the overall heat-transfer into the carcass.

Some value would be held in both Conjugate-Heat Transfer studies and by extending the models to include radiative effects. Large implications on overall heat transfer to the tread may

be found by including these effects. Further, modifications to the rim geometry may be found that may allow for better control over tyre carcass temperatures.

Further trackside investigation or access to data would allow refinement of the boundary conditions to better replicate real-life scenarios. By decreasing Re and conversely increasing Ra during a simulation a more realistic approximation of the heat up of the tread over a braking zone may be replicated. Also by modifying the type of boundary condition, especially the tyre sidewall would hold much value.

Throughout this thesis, minimal change in outer cylinder heat transfer is seen with Reynolds Number and thus control over heat transfer to tyre carcass through wheel internal flow would be difficult to achieve. Development should focus more significantly on the emissivity of rim surfaces and on conjugate heat transfer studies around the tyre bead in particular. Surface roughness and applied coatings to the rim surface to control these properties are most likely to yield future performance benefits in controlling tyre temperature. This document, however, quantifies the implication of internal flows and may further assist more accurate tyre temperature calculations.

5.3 Conclusions

In this research, steady-state and a large timestep transient methodology were utilised with varying efficiencies but a close correlation between both methods. In addition, both natural convection phenomena i.e. zero rotation, on the grid/pitstop scenario as well as a variation in Re were investigated and effect on outer cylinder heat transfer statistics characterised.

Both transient and steady-state methodologies presented were in good quantitative agreement. Minimal variance in normalised temperature was observed in the plume region apart from slight deviation at around $\frac{R-R_i}{L} = 0.05$. Contours of normalised temperature showed similar traits apart from variations in the stagnant region at $\theta > 120°$. Performance statistics were presented with transient methodologies on average taking 0.709% longer per iteration but less time was spent solving linear equations suggesting larger write times occurred. Transient simulations conducted took 51.06% longer than corresponding steady-state methods presented due to the number of iterations required. As solutions tended towards steady-state characteristics, one singular write file at the end of a simulation could reduce the average time per iteration significantly. However, this may be difficult as time histories are not known *a priori*. Therefore, this may only be possible for repeat solutions.

Natural convection phenomena were observed inside a simplified tyre geometry. A thermal

plume along with 2 counter-rotating vortices in the upper section of the annulus drives the flow within the domain. Additionally, 2 spanwise vortices in the upper corners of the domain in the impingement cause local separation along with Nu peaks close to the tyre sidewall. In the centre of the domain, i.e. $0.1 < w < 0.2$, a region of quasi-homogenous thermal effects occurs with minimal oscillation in Nu across this region. Turbulence generation and dissipation were consistent with the presented literature and only occurred in the upper regions of the domain, the inner cylinder boundary layer and the buoyant jet on the outer cylinder wall.

The effect of whole domain rotation on temperature and heat transfer statistics was also investigated. Velocity presented with a linear gradient between inner and outer cylinders or concentric rings in the contour plot. The temperature in all cases presented as relatively well mixed and homogenous and independent of whole domain rotation values. Thermal gradient close to the walls and Nu did have a loose dependency, however, with an approximate 21% variation in outer cylinder Nu between $Re = 4.851 \times 10^5$ and $Re = 1.698 \times 10^6$ cases. However, this was not replicated between $Re = 1.698 \times 10^6$ and $Re = 2.910 \times 10^6$ with almost no variation in outer cylinder Nu.

Appendix

Appendix A: Boundary Conditions

Case	Ra	g	V	omega	U	Re	
1	5.020E+06	-4.50	0	0	0	0	0
2	1.094E+07	-9.81	16.67	49.76119	12.44279	4.85E+05	
3	1.094E+07	-9.81	58.33	174.1194	43.53856	1.70E+06	
4	1.094E+07	-9.81	100	298.5075	74.64179	2.91E+06	

Ro	335	*mm*
Ri	165.1	*mm*
nu	2.56E-05	*m^2/s*
Pr	0.7167	*N/A*
alpha	3.46E-05	*m^2/s*
beta	2.02E-03	*1/K*

References

Bishop, E. (1988). Heat transfer by natural convection of helium between horizontal isothermal concentric cylinders at cryogenic temperature. *Journal of Heat Transfer , Series C)*, *110*(1).

Brembo. (2018). *F1 infographics.* Retrieved from `http://www.brembo.com/en/car/formula-1/f1-infographics`.

CFDOnline. (2014). *Turbulence free-stream boundary conditions.* Retrieved from `https://www.cfd-online.com/Wiki/Turbulence_free-stream_boundary_conditions`.

Chalingé, S. (2011). *Tire thermal analysis and modeling* (Unpublished master's thesis). Chalmers University of Technology.

Char, M., & Hsu, Y. (1998). Numerical prediction of turbulent mixed convection in a concentric horizontal rotating annulus with low-re two-equation models. , *41*.

Collantine Media. (2016). Retrieved from `https://www.racefans.net/wp-content/uploads/2016/10/mercedes-2016-3.jpg`.

Dávid, H. (2017). *Igazi f1-es technikák, egészen közelről: Kina.* Retrieved from `https://hu.motorsport.com/f1/news/igazi-f1-es-technikak-egeszen-kozelrol/#image-scuderia-toro-rosso-str12-rear-wheel-detail-12350152`.

Desai, C., & Vafai, K. (1994). An investigation and comparative analysis of two- and three-dimensional turbulent natural convection in a horizontal annulus. *International Journal of Heat Mass Transfer*, *94*, 2475–2504.

Diasinos, S. (2008). *The aerodynamic interaction of a rotating wheel and a downforce producing wing in ground effect* (Unpublished doctoral dissertation). University of New South Wales, Sydney, Australia.

Fadl, M., He, L., Stein, P., & Marinescu, G. (2017). Assessment of unsteadiness modelling for transient natural convection..

Farouk, B., & Güçeri, S. (1982, 11). Laminar and turbulent natural convection in the annulus between horizontal concentric cylinders. *Journal of Heat Transfer*, *104*, 631–636.

FIA. (2017). *Formula one - sporting regulations - 2018.*

Fluent Inc. (2006, 09). *Fluent 6.3 user's guide* (Tech. Rep.). Fluent Inc.

Formula 1 World Championship Limited. (2015). *Brakes.* Retrieved from `https://www.formula1.com/en/championship/inside-f1/understanding-f1-racing/Brakes.html`.

Formula 1 World Championship Limited. (2018). *What are the new f1 sporting regulations for 2018?* Retrieved from `https://www.formula1.com/en/latest/features/2018/1/what-are-the-new-f1-sporting-regulations-for-2018-.html`.

Francis, N., Itamura, M., S. W., W., & James, D. (2002, 10). *Cfd calculation of internal natural convection in the annulus between horizontal concentric cylinders* (Tech. Rep.). Sandia National Laboritories.

Jongen, T. (1992). *Simulation and modelling of turbulent incompressible flows.* (Unpublished doctoral dissertation). EPF Lausanne, Lausanne, Switzerland.

Kenjereš, S., & Hanjalić, S. (1995). Prediction of turbulent thermal convection in concentric and eccentric horizontal annuli. *Internation Journal Heat and Fluid Flow*, *16*, 429–439.

Kuehn, T., & Goldstein, R. (1976, 1). Correlating equations for natural convection heat transfer between horizontal circular cylinders. *International Journal of Heat and Mass Transfer*, *19*(10), 1127–1134. doi: 10.1016/0017-9310(76)90145-9

Kuehn, T., & Goldstein, R. (1978, 11). An experimental study of natural convection heat transfer in concentric and eccentric horizontal cylindrical annuli. *Journal of Heat Trasnfer*, *100*, 635–640.

Launder, B., & Spalding, D. (1974). The numerical computation of turbulent flows. *Computer Methods in Applied Mechanics and Engineering*, *3*, 269–289.

Milliken, W., & Milliken, D. (1995). *Race car vehicle dynamics* (1st ed.). SAE International.

Motorsport Network. (2015). *Hamilton says mexican gp track is "crazy" slippery.* `https://www.motorsport.com/f1/news/hamilton-says-mexican-gp-track-is-crazy-slippery/`.

Pacejka, H., & Bakker, E. (1992). The magic formula tyre model. *International Journal of Vehicle Mechanics and Stability*, *21*, 1–18.

Padilla, E., & Silvira-Neto, A. (2008). Large-eddy simulation of transition to turbulence in natural convection in a horizontral annular cavity. *International Journal of Heat and Mass Transfer*, *51*, 3656–3668.

Pappone, J. (2017). Tires are the trickiest aspect of formula one, lance stroll says. *Montreal Gazette*. Retrieved from `http://montrealgazette.com/sports/auto-racing/tires-are-the-trickiest-aspect-of-formula-one-lance-stroll-says`.

Patankar, S., & Spalding, D. (1972). A calculation procedure for heat, mass and momentum transfer in three-dimensional parabolic flows. *Internation Journal of Heat and Mass Transfer.*, *15*, 1786–1806.

Rhie, C., & Chow, W. (1983). Numerical study of the turbulent flow past an airfoil with trailing edge separation. *AIAA Journal*, *21*(11), 1525–1532.

Sprot, A. (2013). *Open-wheel aerodynamics: Effect of tyre deformation and internal flow* (Unpublished doctoral dissertation). Durham University.

Thermal-Fluids Central. (2010). Retrieved from `https://www.thermalfluidscentral.org/encyclopedia/index.php/Thermophysical_Properties:_Nitrogen_at_1_atm`.

thisisf1.com. (2017). *Battle for 6th – angry toro rosso hit back at renault over engine failures.* Retrieved from `https://www.thisisf1.com/2017/11/11/battle-for-6th-angry-toro-rosso-hit-back-at-renault-over-engine-failures/`.

Tu, J., Yeoh, G., & Liu, C. (2013). *Computational fluid dynamics: A practical approach* (2nd ed.). Butterworth-Heinemann.

Van Leer, B. (1979). Towards the ultimate concervative difference scheme. iv. a second order sequel to godunov's method. *Journal of Compuational Physics*, *32*, 101–136.

Versteeg, H., & Malalasekera, W. (2007). *An introduction to computational fluid dynamics: The finite volume method* (2nd ed.). Pearson Education Limited.

Wischnewski, B. (2018). Retrieved from `http://www.peacesoftware.de/einigewerte/stickstoff_e.html`.

Wolfstein, M. (1969). The velocity and temperature distribution of one-dimensional flow with turbulence augmentation and pressure gradient. *Internation Journal of Heat and Mass Transfer.*, *12*, 301–318.

Yakhot, V., & Orzag, S. (1986). Renormilization group analysis of turbulence: I. basic theory. *Journal of Scientific Computing*, *1*(1), 1–51.

Yang, X., & Olatunbosun, O. (2011). Optimization of reinforcement turn-up effect on tyre durability and operating characteristics for racing tyre design. *Journal of Materials and Design*, *35*, 798–809.